Solar Phys (2008) 253: 3–41
DOI 10.1007/s11207-008-9258-9

Radio Emission of Flares and Coronal Mass Ejections

Invited Review

A. Nindos · H. Aurass · K.-L. Klein · G. Trottet

Received: 25 April 2008 / Accepted: 16 August 2008 / Published online: 4 October 2008

Abstract We review recent progress on our understanding of radio emission from solar flares and coronal mass ejections (CMEs) with emphasis on those aspects of the subject that help us address questions about energy release and its properties, the configuration of flare – CME source regions, coronal shocks, particle acceleration and transport, and the origin of solar energetic particle (SEP) events. Radio emission from electron beams can provide information about the electron acceleration process, the location of injection of electrons in the corona, and the properties of the ambient coronal structures. Mildly relativistic electrons gyrating in the magnetic fields of flaring loops produce radio emission via the gyrosynchrotron mechanism, which provides constraints on the magnetic field and the properties of energetic electrons. CME detection at radio wavelengths tracks the eruption from its early phase and reveals the participation of a multitude of loops of widely differing scale. Both flares and CMEs can ignite shock waves and radio observations offer the most robust tool to study them. The incorporation of radio data into the study of SEP events reveals that a clear-cut distinction between flare-related and CME-related SEP events is difficult to establish.

Keywords Sun · Flares · Coronal mass ejections · Radio radiation · Corona

Radio Physics and the Flare-CME Relationship
Guest Editors: Karl-Ludwig Klein and Silja Pohjolainen.

A. Nindos (✉)
Section of Astrogeophysics, Physics Department, University of Ioannina, Ioannina 45110, Greece
e-mail: anindos@cc.uoi.gr

H. Aurass
Astrophysikalisches Institut Potsdam, 14482 Potsdam, Germany
e-mail: haurass@aip.de

K.-L. Klein · G. Trottet
Observatoire de Paris, LESIA – CNRS UMR 8109, 92190 Meudon, France

K.-L. Klein
e-mail: ludwig.klein@obspm.fr

G. Trottet
e-mail: gerard.trottet@obspm.fr

1. Introduction

Flares and coronal mass ejections (CMEs) are the most violent phenomena in the solar system. Flares involve the catastrophic release of magnetic energy in the low corona, through magnetic reconnection. In a typical flare, plasma is heated and particles are accelerated to relativistic energies on short time scales. A large flare may result in the acceleration of 10^{37} electrons per second to energies > 20 keV for periods of tens of seconds. The energy release in a flare is characterized normally by two phases: an impulsive phase and an extended (decay) phase.

A CME is the expulsion of coronal plasma and magnetic field entrained therein into the heliosphere. The event is detected by coronagraphs in white light; however, the initiation and early stages of the event are not visible by coronagraphs and observations from other instruments must be employed. In an average event, $10^{14} - 10^{16}$ g of material is ejected into the heliosphere with speeds ranging from 100 to 2000 km s^{-1}.

CMEs have a strong association with flares and erupting filaments and prominences. Flares happen in active regions whereas filaments are observed both in active regions and on the quiet Sun. However, there is no one-to-one association between flares and CMEs. CMEs are large-scale eruptions and when they are associated with flares these flares are called "eruptive flares" whereas flares without CMEs are called "confined flares." In CMEs the bulk of the released energy is mechanical, whereas flares result from a local release of energy in the low corona, with the bulk of the energy going into prompt particle acceleration and plasma heating. CME kinematics and the energy release of the associated flare are closely related (*e.g.*, Zhang *et al.*, 2001), implying that both phenomena are different manifestations of magnetic energy conversion in the corona (*e.g.*, Harrison, 1995).

Flare- and CME-associated phenomena produce radio waves in a frequency range that may cover more than seven orders of magnitude from a few tens of kHz (close to the Earth) to a few tens or hundreds of GHz (in the chromosphere). The radio spectrum provides rich diagnostic potential because two of the natural frequencies of the solar atmosphere, the electron plasma frequency, $\omega_{\mathrm{p_e}}$, and the electron gyrofrequency, ω_{B_e}, are in the radio band. The sensitivity of radio emissions to coronal magnetic field and the properties of nonthermal particles make them a unique tool for the understanding of processes associated with flares and CMEs. Synergies between radio diagnostics and information provided by optical, (E)UV, soft X-ray (SXR), and hard X-ray (HXR) data provide unprecedented opportunities for the development of a unified, global view of solar flares and CMEs.

In this article we review some of the basic properties of radio emission of flares and CMEs with emphasis on those which, in our opinion, have something to tell us about the underlying physics of the phenomena. Therefore we do not pretend that we exhaust the subject. Our article is organized as follows. After summarizing the basic solar radio emission mechanisms, we discuss in Section 3 radio emission from electron beams; radio emission from electrons trapped in flaring loops is addressed in Section 4. In Section 5 radio fine structures associated with electron acceleration episodes are considered. In Section 6 we address CME-associated radio emission, and in the last two sections we discuss what radio data can tell us about shocks and solar energetic particles.

2. Emission Mechanisms and Propagation Effects

The Faraday depth of the corona is extremely large and the relevant Stokes parameters are I and V, the total intensity and circular polarization, respectively. Before radio waves reach

the Earth, they travel through the magnetized coronal and heliospheric plasma, which may absorb or emit and/or refract or reflect the radiation and/or change its polarization. Thus the properties of observed radio emission depend on (1) the emission mechanism(s) at the region of formation of the radiation and (2) radiative transfer and propagation effects.

2.1. Emission Mechanisms

Radio emission may originate from electrons having either a thermal or a nonthermal distribution, and the emission mechanisms can be either incoherent or coherent. In incoherent mechanisms, there is no back-reaction of the emission on the particle distribution, and the photons emitted, whose number is proportional to the number of particles, have no phase association. In coherent mechanisms the electrons all undergo acceleration in phase, acting together to produce photons that are in phase. The brightness temperature resulting from a coherent emission mechanism can thus largely exceed the mean energy of the emitting particles.

A magnetic field renders a plasma "birefringent" and thus the intrinsic polarization at the region of formation of the radio emission is determined by the predominant emission mode, extraordinary (x-mode) or ordinary (o-mode) and the polarization characteristics of that particular mode. (In the corona the z-mode and whistler mode cannot propagate from the source to infinity owing to stopbands in the refractive index.)

2.1.1. Incoherent Mechanisms

The two most important incoherent mechanisms are free-free emission (bremsstrahlung) and gyroemission.

- *Free-free emission* is produced when electrons are deflected in the Coulomb field of ambient ions owing to the acceleration they experience by the Coulomb force. When the electrons are part of a nonthermal distribution, emission usually occurs at HXRs when the encounters are close. When the electrons and ions belong to the same thermal distribution, Coulomb interactions are weaker and emission is produced at radio wavelengths. Then the opacity is proportional to $N_{\rm e}^2 T_{\rm e}^{-1.5} f^{-2}$ (where $N_{\rm e}$ and $T_{\rm e}$ are the electron density and temperature, respectively, and f is the frequency of observation). Typically, in a magnetized plasma thermal free-free emission is weakly polarized in the sense of the x-mode. The optically thin spectrum of free-free emission is flat, so practically the same flux is produced at all wavelengths. In principle, the hot coronal plasma that fills flaring loops emitting SXRs will also radiate in the decay phase at centimeter and millimeter wavelengths owing to optically thin free-free emission (*e.g.*, Kundu and Vlahos, 1982).
- *Gyroemission* originates from electrons accelerated in the presence of a magnetic field: As they experience the Lorentz force, they emit radiation at the harmonics of the electron gyrofrequency. For thermal coronal electron distributions in a homogeneous magnetic field the absorption coefficient at low harmonics has a line spectrum (gyroresonance emission). At mildly relativistic speeds (electron energies of tens of keV to a few MeV) the radiation pattern emitted by a single electron gets increasingly beamed and it emits at higher harmonics of the electron gyrofrequency, typically from ten to a few hundreds. For an ensemble of emitting electrons the bandwidth of each harmonic increases owing to both thermal broadening and the energy spread of the electron distribution function. These effects yield a quasi-continuum emission over a wide frequency band. This form of emission is called gyrosynchrotron emission and is the basic microwave process operating in flares.

Unlike X-ray radiation, gyrosynchrotron radiation is sensitive to magnetic field strength and orientation. It also depends on the energy and pitch-angle distribution functions of the energetic electrons, the density of the ambient plasma, and the frequency of observation (see Ramaty, 1969; Fleishman and Melnikov, 2003a, 2003b, for the complete expressions). For large ambient densities the index of refraction departs significantly from unity at low frequencies, resulting in the suppression of intensity (Razin effect). The emission coefficient is larger for the x-mode than for the o-mode, whereas the inverse is true for the source function. Thus the polarization of an optically thin region is that of the x-mode, whereas an optically thick region will have o-mode polarization. Circular polarization can be significant when the source is viewed along the magnetic field direction, and opacity is maximized when the source is viewed orthogonal to the magnetic field direction.

In addition to these mechanisms, *transition radiation* can result from a variation in phase speed of wave propagation at transition boundaries (Ginzburg and Frank, 1946). It may arise whenever nonthermal particles pass through small-scale inhomogeneities (*e.g.*, wave turbulence). Usually it is weak, but Platonov and Fleishman (1994) showed that its intensity can be greatly enhanced by plasma resonance at frequencies just above the local plasma frequency.

2.1.2. Coherent Mechanisms

Coherent radio emission is driven by kinetic instabilities of unstable particle distribution functions f. The two most important coherent mechanisms are plasma emission (see Melrose, 1987, for a review) and electron cyclotron maser emission.

- *Plasma emission.* In the corona the propagation of electron beams and/or shocks can excite plasma emission, which is electromagnetic radiation emitted at the plasma frequency $f_{\mathrm{pe}} = 9\sqrt{N_{\mathrm{e}}}$ (with f_{pe} in kHz and N_{e} in cm^{-3}) and its second harmonic ($2f_{\mathrm{pe}}$). It is a three-step process:

  1. *Beam formation*: If the acceleration itself does not produce a beam, propagation will: Faster particles will outpace slower ones, yielding a bump in the tail of the original distribution function.
  2. *Plasma instability*: The bump distribution has positive slope $\partial f/\partial v_{\parallel} > 0$ (where $v_{\parallel}$ is the particle's velocity parallel to the magnetic field), which is unstable to the production of Langmuir waves: The positive slope is a source of free energy, and Langmuir waves can grow at the expense of the electron energy. The most crucial problem is the evolution of the bump-on-tail instability. Traditionally (*e.g.*, Benz, 1993), it is believed that the bump distribution relaxes into a plateau (but see Robinson, Cairns, and Gurnett, 1992, for an alternative approach applying to a strongly inhomogeneous medium).
  3. *Wave conversion*: The Langmuir waves can be transformed in part into electromagnetic waves at the plasma frequency and its harmonic via scattering off thermal ions or, more likely, coupling to low-frequency waves (*e.g.*, ion-acoustic waves). The generation of radio radiation can be understood in terms of the conservation of momentum and energy. Plasma emission is obtained when a conversion into an electromagnetic wave occurs.

  Plasma radiation is heavily damped by collisional opacity and so this emission is typically seen only at low frequencies (*i.e.*, low densities) or when the ambient plasma is very hot.

Emission at the fundamental of the plasma frequency should be 100% polarized in the sense of the *o*-mode because the *x*-mode is cut off at a frequency above $f_{\rm pe}$. However, such high degrees of circular polarization of plasma radiation are not frequently observed because of propagation effects (Melrose, Robinson, and Feletto, 1995). Harmonic plasma emission is also polarized in the sense of the *o*-mode (*e.g.*, Zlotnik, 1981).

- *Electron cyclotron maser emission.* In plasmas where $\omega_{B_{\rm e}} \gg \omega_{\rm pe}$ the pitch-angle anisotropy will transfer energy into directly escaping electromagnetic radiation with frequency ω and wave number k when the condition $\omega - k_{\parallel} v_{\parallel} = s\omega_B$ is satisfied, where s is the harmonic number (see Melrose, 1997, for a review).

2.2. Propagation Effects

The refractive index of an unmagnetized plasma is given by $n = \sqrt{1 - (\omega_{\rm pe}/\omega)^2}$, which, at low frequencies, can be significantly smaller than unity, and the radio emission eventually will suffer total reflection when $\omega = \omega_{\rm p}$. Generally, refraction effects are not important unless the optical depth between the observer and the point of total reflection is small. Refraction and total reflection effects are more serious in the presence of large-scale density gradients in the background corona and solar wind (*e.g.*, streamers, coronal holes, and fast or slow solar wind streams). This can result in apparent position offsets and/or distortions of the radio brightness distribution (*e.g.*, Duncan, 1979; Lecacheux *et al.*, 1989; Mercier, 1996). Furthermore, ionospheric refraction can significantly perturb the apparent position of a source in ground-based observations, sometimes exceeding several arcminutes in the 100 – 300 MHz frequency range. In the presence of small-scale inhomogeneities between the radio source and the observer, a variety of scattering phenomena may occur. These include angular and spectral broadenings, resulting in a frequency-dependent blurring in radio maps (*e.g.*, Bastian, 1994).

Under the geometrical optics approximation (not too low values for the electron density and magnetic field), the *x*- and *o*-mode waves are polarized in opposite senses and when the physical conditions change along the ray path, its polarization will change accordingly. This implies that when the wave crosses a transverse field region (TFR), the sense of polarization will change because the sign of the longitudinal component of the magnetic field changes. This picture is valid when the *x*- and *o*-mode waves propagate independently (weak coupling). However, when the waves are strongly coupled their polarization remains fixed, even if a TFR is crossed (Cohen, 1960; Zheleznyakov, 1970). Therefore, circular polarization observations do not necessarily reflect the magnetic field polarity at the source of the emission (*e.g.*, Alissandrakis and Preka-Papadema, 1984; Alissandrakis, Nindos, and Kundu, 1993).

3. Electron Beams

3.1. Metric and Decimetric Emissions

Beams of energetic electrons can produce radio emission at the local plasma frequency or its harmonic via the plasma mechanism. In dynamic spectra the bursts appear as intense bands of emission drifting rapidly to low or high frequencies depending on whether the beams travel along regions of negative or positive ambient coronal density gradient (*i.e.*, away or toward the Sun, respectively). Bursts drifting to lower frequencies are called type III bursts whereas those drifting to higher frequencies are called reverse-drift or reverse-slope (RS) bursts. Type III bursts are seen to propagate out to regions of very low density

and therefore the exciter corresponds to radio-emitting beams that escape upward along open magnetic field lines. Bidirectional type III bursts have been observed, consisting of separate components that drift both up and down in frequency from a common origin (Aschwanden, Benz, and Schwartz, 1993). Since the drift in frequency with time can be directly converted into a drift of ambient coronal density with height, the beam velocity can be computed if a coronal density model is provided. Generally the speeds derived are about $0.1c - 0.2c$, which correspond to kinetic energies of a few to 10 keV for type-III-emitting electrons (*e.g.*, Aschwanden, 2002).

Beams of energetic electrons may propagate along closed field lines and thus in a dynamic spectrum they first show a negative frequency drift rate and later, after they cross the loop's apex, a positive one. In dynamic spectra such radio-emitting electrons show an inverted U shape and are called U-bursts (*e.g.*, Aschwanden *et al.*, 1992; Aurass and Klein, 1997).

As the height increases, the lower opacity and the beam-focusing effect of the decreasing magnetic field makes the detection of radio emission from electron beams easier. Therefore it is not surprising that in most cases, at least at meter wavelengths, normal type IIIs are observed. However, above 1 GHz one sees mainly RS bursts, which indicates that they are associated with electron beams in closed loops that propagate downward, away from acceleration regions. At around 500 MHz, it is roughly equally possible to observe a normal type III or an RS burst (*e.g.*, Isliker and Benz, 1994). At decimeter and centimeter wavelengths free-free absorption plays a significant role, but its influence can be overcome if the bursts are due to harmonic plasma radiation and the radio sources are located in overdense structures featuring high temperature and/or small density scale height (Trottet *et al.*, 1982; Aschwanden *et al.*, 1985; Robinson and Benz, 2000).

Only a very small number of coronal type III events appear isolated on the dynamic spectra. Usually, type IIIs appear in groups (see Figure 1, lower panel) of some ten or more bursts and are commonly seen in the impulsive phase of flares. Occasionally, however, they may appear at times when there is no activity at other wavelengths. The question of whether the acceleration and injection of component type-III-producing electrons is coherently modulated in a single source or is driven by a statistical flare (*e.g.*, Vlahos *et al.*, 1995) in a spatially fragmented energy release site has been debated extensively. In several cases type IIIs appear not randomly but in quasi-periodic time intervals, which has been interpreted (*e.g.*, Aschwanden, Benz, and Montello, 1994) in terms of a large-scale mechanism, responsible for the modulation of the beam injection affecting the whole active region. However, Isliker (1996) pointed out that the quasi-periodicity criterion utilized by Aschwanden, Benz, and Montello (1994) is inadequate because its spread is such that periodic and stochastic behavior overlap significantly. However, in the framework of the fragmented acceleration site model (*e.g.*, Vlahos, 1994) the components of the type III group are excited by electrons propagating along different flux tubes, each rooted in a source element (Benz, Jaeggi, and Zlobec, 1982; Pick and van den Oord, 1990; Vlahos and Raoult, 1995). The work by Hillaris *et al.* (1999), who extrapolated observed flux–time profiles of type IIIs toward higher frequencies and estimated the injection time for the individual radio-emitting beams, is consistent with trends appearing in simulations of the statistical flare (*e.g.*, Vlahos *et al.*, 1995).

Type IIIs often appear much higher than would be expected on the basis of coronal density models. This may be due to the influence of refraction effects, which lead to a displacement of the observed apparent source positions, or due to their preferential emanation from overdense coronal structures. Statistical results support the former interpretation (*e.g.*, Poquérusse *et al.*, 1988), but the occasional association of type IIIs with weak SXR jets (*e.g.*, Aurass, Klein, and Martens, 1994; Raulin *et al.*, 1996) might indicate

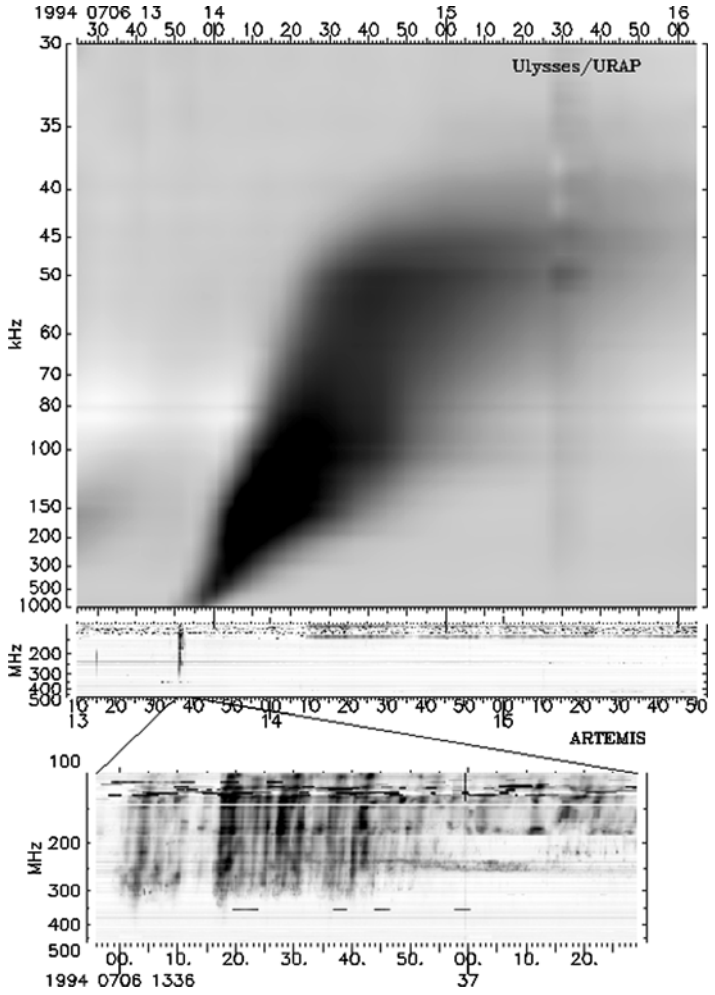

Figure 1 Artemis observations of a group of coronal type III bursts (middle panel) and the corresponding IP type III radio burst from *Ulysses* (top panel). The bottom panel shows the fine structure of the group of the coronal type III bursts (from Poquérusse *et al.*, 1995).

that some type IIIs occur in overdense structures. In principle, magnetic field extrapolations can also be used for back-tracking the radio emission (*e.g.*, Aschwanden *et al.*, 1992; Yan *et al.*, 2006).

3.1.1. Relationship with Hard X-Rays

Because of their different emission mechanisms and source regions, radio emission from beams and HXRs is often observed in the same flare but in general they do not correlate well. Because nonthermal HXR bremsstrahlung is mostly produced by precipitating electrons in the chromosphere, one expects that the most frequent radio counterpart should show RS bursts (Aschwanden *et al.*, 1985). As the start frequency of the radio-emitting electrons decreases, their correlation with HXRs becomes poorer probably because most of them are

metric type IIIs that propagate upward. Overall, in most flares the number of type IIIs or RS bursts exceeds the number of HXR peaks. Recent statistical results by Benz *et al.* (2005) do not modify radically the earlier findings: They found that some 17% of flares do not show radio emission in meter and decimeter wavelengths. But in almost all of the HXR flares associated with some kind of coherent radio emission, type IIIs or/and RS bursts were detected. A majority of 72% of them occur in the decimeter wavelength range and less than 10% of these continue to meter waves. Classic meter-wavelength type IIIs are associated in 33% of all HXR flares, but only in 4% of HXR events are metric type IIIs the only observed emission. They also find type III emissions in 9% of the flares well before (up to 5 min) the HXR emission started.

When, as in most cases, type III emission is associated with the impulsive phase of the flare, there is a delay of the radio emission with respect to the HXR emission (*e.g.*, Aschwanden, Benz, and Schwartz, 1993; Arzner and Benz, 2005). The cause of the radio delay has been attributed to the lower energy of the radio-emitting electrons, the growth time for Langmuir waves, and scattering near the source region.

3.1.2. Implications for Flare Models

The so-called standard model for eruptive long-duration flares invokes a helmet streamer configuration in which closed-loop field lines lie under a monolithic current sheet. In it (*e.g.*, Shibata *et al.*, 1995) no open field lines are shown. Other models applied to impulsive flares involve interactions between pairs of closed loops. The outcome of reconnection is two new closed loops, making it difficult to see how type IIIs could originate in the energy-release region. For flares with a good temporal and spectral correlation with electron events observed *in situ*, the flare geometry indeed looks different. These events show hot flare loops with HXR footpoints, plus an additional HXR source separated from the loop by $15''$. This source structure can be explained by a simple magnetic reconnection model with newly emerging flux tubes that reconnect with previously open field lines (so-called interchange reconnection). The previously open field lines form the flaring loops, whereas heating along the newly opened field lines is weaker because material can easily be lost because of the open geometry of the field. Type-III-producing electrons escape along the newly opened field line.

The fact that type IIIs occasionally appear in the preflare phase (*e.g.*, Benz *et al.*, 1983; Raoult *et al.*, 1985) indicates the presence of electron acceleration in it. Furthermore, in the study by Benz *et al.* (2005) such events are often accompanied by the emission of a thermal source in the corona before the appearance of the HXR emission from the footpoints. These observations may imply that the energization process that operates in the preflare phase is mostly heating coronal plasma and possibly driving evaporation by conduction. Its efficiency in particle acceleration is very limited. This is consistent with stochastic acceleration operating on the thermal particle population. It can accelerate particles to nonthermal velocities only if acceleration is faster than collisions.

The start frequency of the radio emission from electron beams is one of the best probes of the electron acceleration region. The occasional tight correlation between upward- and downward-directed beams of electrons in the corona (*e.g.*, Aschwanden *et al.*, 1995) has been used for the diagnosis of the acceleration region. Aschwanden and Benz (1997) inferred the ambient coronal density of the acceleration region, $N_{\rm acc}$, from the plasma frequency at the separatrix between correlated type III bursts and RS bursts: They found that $N_{\rm acc} = (0.6-10) \times 10^9$ cm^{-3}, which was much lower than in the associated bright SXR flaring loops (where $N_{\rm e} = (0.2-2.5) \times 10^{11}$ cm^{-3}). This is not contradictory, since the X-ray source

becomes bright as a consequence of chromospheric evaporation (*i.e.*, several minutes after the start of the impulsive energy release). The observations were interpreted as evidence that reconnection occurs in a cusp geometry above the flaring loops. This is consistent with electron time-of-flight studies from HXRs (Aschwanden, 2002) as well as with geometries inferred from HXR above-the-loop-top sources. But in the framework of the chromospheric evaporation scenario one should not expect that such dense loops already exist when the electrons carrying the bulk of the released energy start to be accelerated.

The standard model, however, shows problems. The most serious in the framework of our discussion is the so-called number problem: For a typical flare more than 10^{39} electrons will be accelerated, yielding a huge current sheet (with a volume of $\sim 10^{28}$ cm^3) that should remain stable for more than 1 minute. This is difficult to imagine and indeed the dissolution of the current sheet and the formation of several smaller fragments will be its natural evolutionary path (*e.g.*, Kliem, Karlický, and Benz, 2000).

A popular mechanism is stochastic acceleration by the magnetic field component of low-frequency waves. In it, particles near Cerenkov resonance are mirrored by the waves. High-frequency waves near the plasma frequency can be excluded as drivers for this model, as they would couple into decimeter waves and be present in every flare, which is not the case. This model is not in disagreement with the occasional lack of coherent radio emission from some flares because the frequency of the postulated turbulence is far below the plasma frequency and does not cause radio emission. However, discrepancies of the model with the observed shape of HXR spectra have been reported.

3.2. Interplanetary Type III Bursts

Type III bursts in the interplanetary medium can be grouped into three broad classes: (1) isolated type III bursts, (2) type III storms, and (3) complex type III bursts.

3.2.1. Isolated Interplanetary Type III Bursts

Isolated interplanetary (IP) type III bursts are the most common class of type III bursts in the IP medium. They are related to flares and small-scale energy-release episodes in the low corona and indicate the propagation of electron beams along open magnetic field lines that extend into the IP medium. Because of velocity dispersion the groups of electron beams usually observed in the corona merge into one broad beam in the IP medium.

Studies of the correlation between IP and coronal type III bursts (Poquérusse *et al.*, 1995) reveal that in several cases groups of coronal type III bursts are related to most IP type III bursts whose spiral field lines are rooted in the visible side of the Sun. An example appears in Figure 1, which shows a composite dynamic spectrum consisting of ground-based (Artemis) and space-borne (*Ulysses*) radio data: The extrapolation of the slope of the leading edge of the IP type III emission down to the frequencies of the coronal band shows that the origin of the IP type III burst coincides with the end of the coronal type III group. However, not every solar type III burst, even if strong, produces an IP type III burst.

When one has a way of observing the direction of arrival of the radio waves, the trajectories of the electron beams can be traced from high to low frequencies, hence from the Sun to near the Earth, provided that one assumes a heliospheric density model. Such trajectories have been used to directly confirm the global Parker spiral structure of the IP magnetic field (*e.g.*, Fainberg and Stone, 1974). However, the determination of the radio source locations is complicated by scattering and refraction of the radiation by density inhomogeneities in the IP medium (*e.g.*, Lecacheux *et al.*, 1989) that can strongly affect the

apparent azimuthal positions of the radio source and source angular size, as well as introduce anomalous propagation time delays (*e.g.*, Steinberg *et al.*, 1984). The only way to avoid using a heliospheric density model and track the apparent source directly is by using stereoscopic radio experiments. Until the launch of the two STEREO spacecraft only a small number of such studies had been published (*e.g.*, Caroubalos, Poquérusse, and Steinberg, 1974; Gurnett, Baumback, and Rosenbauer, 1978; Reiner *et al.*, 1995).

3.2.2. Type III Storms

A type III storm is weak dekametric-to-kilometric radio burst activity that typically lasts for days to weeks and consists of thousands of individual short-lived type-III-like bursts in rapid succession. They are produced by low-energy electrons (≈ 2 keV) that are injected from quasi-stable active regions on the Sun and propagate along the magnetic field lines through IP space (Potter, Lin, and Anderson, 1980). Type III storms are known to be associated with metric type I bursts, which in turn are associated with solar active regions. Type I bursts are a non-flare-related phenomenon, consisting of a continuum component and a burst component. The continuum, also often referred to as a "noise storm" (see Elgarøy, 1977; Kai, Melrose, and Suzuki, 1985, for reviews), typically covers the frequency range 40 – 400 MHz, with variations on time scales of hours. Type III storms generally cease, or greatly diminish in intensity, at the time of major CMEs linked to the associated active region (Reiner *et al.*, 2001). After disruption, the type III storms often return to the original level. The storm recovery may require a time of about 10 – 15 hours. The response of type III storms to CMEs is consistent with reported sharp decreases of metric noise storms associated with CMEs (Chertok *et al.*, 2001).

3.2.3. Complex Type III Bursts

These are hectometric type III bursts with high intensities and long durations that occur in groups after (typically about 10 minutes or so, during type II emission) the impulsive phase of flares. These events were first reported by Cane *et al.* (1981) and Cane and Stone (1984), who named them "shock-accelerated" (SA) events and interpreted them as the result of merging of low-frequency extensions not of metric type III but of the herringbone structure of type II bursts (see Section 7.1). In the 1990s the question of whether these bursts come from electrons accelerated in type II burst shocks or are due to flare electron acceleration was confronted with statistical studies. Contradictory results were reported and the issue was not settled (*e.g.*, Kahler, Cliver, and Cane, 1989; MacDowall, Stone, and Kundu, 1987; Kundu, MacDowall, and Stone, 1990; Klein, 1992; Reiner *et al.*, 2000; Dulk *et al.*, 2000).

Cane, Erickson, and Prestage (2002) realized that complex type III bursts show a very high degree of association with solar energetic particle (SEP) events (see Section 8) and introduced the term "type III-*l* bursts" to replace the previous "SA events" term. An example is shown in Figure 2, where type-II-like features (indicated by the black arrows) show up below 30 MHz whereas the type III emission starts at 13:57 UT. Successive packets of type-III-like emission (presumably the type III-*l* bursts; indicated by the white arrows) show up later, starting at successively lower frequencies. Pick and Maia (2005) have argued that type III-*l* bursts are related to sudden changes in the radio emission observed at metric and decametric wavelengths, in particular the onset of new emitting sources at positions that can be at large distances from the flare site. The topic of complex type III bursts remains controversial and it is further discussed in Section 8 in the framework of SEPs.

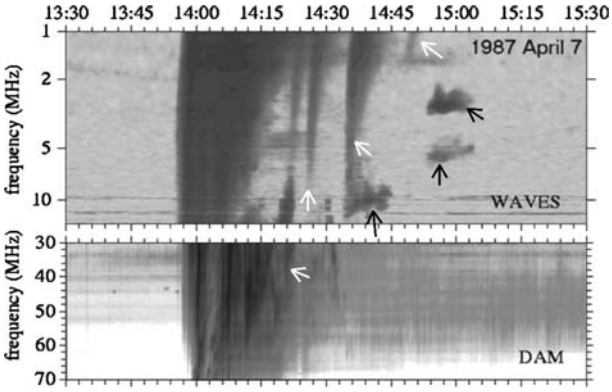

Figure 2 Composite dynamic spectrum of an event combining *Wind*/WAVES and Nançay DAM data. The white arrows point to type III-*l* bursts; the black arrows point to a possible type II burst (from Pick and Maia, 2005; reprinted with permission). The event was observed on 7 April 1997; the date label in the figure was left as it appeared in the article.

4. Radio Emission from Trapped Electrons

4.1. Impulsive Phase Emissions

4.1.1. General Remarks

In the impulsive phase of flares, energetic electrons (with energies of tens to several hundreds of keV) gyrating in coronal magnetic fields of flaring loops produce microwave emission via the gyrosynchrotron mechanism (see reviews by Alissandrakis, 1986; Bastian, Benz, and Gary, 1998). This mechanism is very efficient and allows us to detect electrons with energies of hundreds of keV even in small flares. In addition, recently, gyrosynchrotron emission from nonthermal electrons has been detected in the preflare phase of an event (Asai *et al.*, 2006).

In its simplest form the spectra of microwave bursts in most cases show an inverted U morphology, peaking at a frequency $\nu_{\rm pk} = 5-10$ GHz (see Bastian, Benz, and Gary, 1998, for details and Nita, Gary, and Lee, 2004, for more recent results). The spectrum's peak divides it into roughly two parts: The low-frequency part corresponds to optically thick emission, and the high-frequency part corresponds to optically thin emission. To a first approximation, the morphology of microwave flare emission depends on the magnetic field configuration (*i.e.*, the geometry of the flaring region and its location on the disk) and the properties of the nonthermal electrons. High-spatial-resolution microwave observations of flares have revealed a variety of morphologies. When the flare configuration is simple, the general tendency is that observations at high frequencies show compact sources, presumably associated with the footpoints of flaring loops, whereas at low frequencies there is a tendency for more extended sources, indicating emission from the entire loop that peaks close to the loop top (see Figure 3, top panel). This picture is consistent with the properties of the gyrosynchrotron mechanism: The magnetic field is much stronger near the footpoints of the loop, which favors the higher frequencies (*i.e.*, at a given frequency, higher energy electrons emit at the loop top whereas lower energy electrons emit at the footpoints). A decrease of the frequency of observation has approximately the same effect for the microwave flare emission as an increase of the magnetic field. Thus when the frequency of observation decreases, we expect to have emission not only from the footpoints but also from a significant part of the flaring loop.

Inhomogeneous models of the microwave spatial structure of flaring loops have been computed by Alissandrakis and Preka-Papadema (1984), Klein and Trottet (1984), Preka-Papadema and Alissandrakis (1988, 1992), and Bastian, Benz, and Gary (1998). All of them

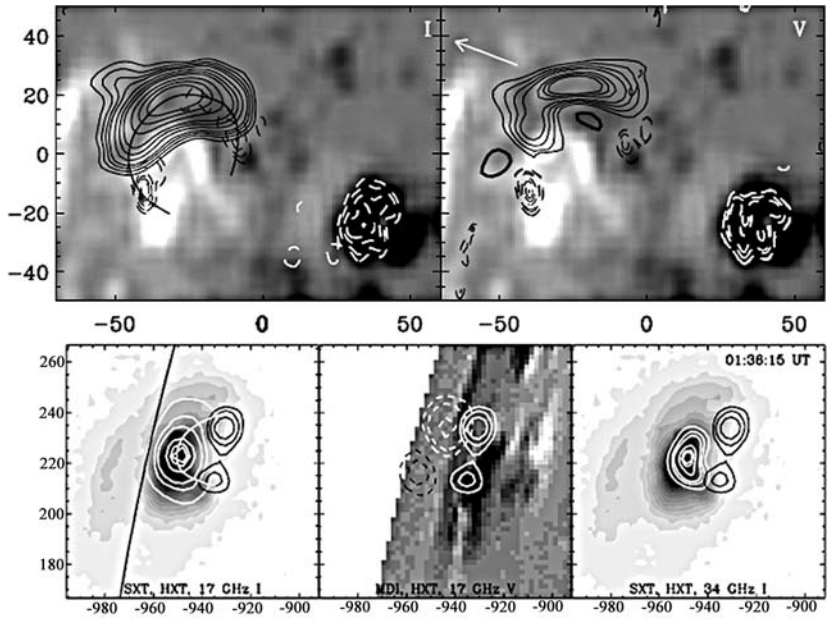

Figure 3 Top row: The 1 July 1992 flare. Contour plots of flare radio emissions observed by the VLA at the time of maximum overlaid on a Kitt Peak photospheric magnetogram. The *I* maps are on the left, and the *V* maps on the right. The solid contours show the 5-GHz emission, and the dashed contours show the 15-GHz emission. In the 5-GHz *V* map the thick contours represent positive brightness temperatures. The white contours in both images show the sunspot-associated emission at 15 GHz. The axes' labels denote seconds of arc from the VLA phase-tracking center. The white arrow indicates the direction of the limb. (Reprinted with permission from Nindos *et al.* (2000).) Bottom row: The 12 January 2000 flare. The left and right panels show a postflare SXT image with white contours showing the 17- and 34-GHz *I* emission at the time of maximum (marked in the right top corner). The middle panel shows an MDI photospheric magnetogram, with the dashed black and dashed white contours denoting the 17-GHz negative and positive *V* emissions, respectively. In all three panels the thick solid contours show the HXR emission from the 33 – 53 keV channel at the time of maximum. The axes' labels denote seconds of arc from disk center. (Reprinted with permission from Kundu *et al.* (2001b).) In the left panels of both rows, the smooth curves delineate the flaring loops, and the thick black curve in the bottom row shows the radio limb.

give a satisfactory qualitative interpretation of the elementary loop burst emission just described. Nindos *et al.* (2000) and Kundu, Nindos, and Grechnev (2004) compared spatial and spectral observations of two microwave bursts at their peak intensity with models of gyrosynchrotron loop emission. In both events, their best-fit models were able to reproduce the observed features of the radio emissions and derive self-consistently several of the properties of the magnetic field and energetic electrons of the flaring loops.

Simultaneous morphological studies of flares in HXRs, SXRs, and microwaves, together with photospheric magnetograms, have provided valuable information about the flare configuration (see, *e.g.*, Alissandrakis, Schadee, and Kundu, 1988, for early results). The interested reader may refer to the review by Bastian, Benz, and Gary (1998) for details. Here we only mention the articles by Nishio *et al.* (1997) and Hanaoka (1996, 1997), who found that the microwave sources arise from interacting loops of widely differing scale. Furthermore, configurations involving more complex loop systems have also been revealed (*e.g.*, Kundu *et al.*, 1982, 2004). Note that, generally, microwave images have higher dynamic ranges than

the one provided by today's HXR instrumentation and thus in several cases the microwave images show more sources than the corresponding HXR images.

4.1.2. Trapping and Precipitation

Most of the comparisons between HXR and microwave flare emissions have been discussed in the framework of the "direct precipitation/trap plus precipitation" (DP/TPP) model (*e.g.*, Bastian, Benz, and Gary, 1998; Aschwanden, 2002; and references therein). Briefly, energetic electrons with small pitch angles are guided by the magnetic field directly to the chromosphere, where they are stopped by relatively cool, dense material. Most of their energy goes into heating the ambient chromospheric plasma but a fraction is emitted radiatively via nonthermal thick-target bremsstrahlung as HXRs. Electrons with larger pitch angles are trapped by coronal magnetic fields and emit nonthermal gyrosynchrotron radiation. Eventually they are scattered into the loss cone via Coulomb collisions or wave – particle interactions (and if the Razin effect is observed together with the spectral flattening, this may provide additional evidence for the importance of Coulomb collisions) and precipitate out of the magnetic trap, producing additional HXRs.

Historically, the TPP scheme has been used to deal with the effect of Coulomb collisions on the electron energy. More energetic electrons suffer fewer collisions than less energetic ones, and therefore they have longer lifetimes in the trap. In this way one can understand the frequency-dependent time delays between microwave peaks, the usual microwave lag behind the time of HXR maximum flux, and the slower decay of microwave emission than that of HXR emission (*e.g.*, Bruggmann *et al.*, 1994; Melnikov and Magun, 1998; Bastian, Benz, and Gary, 1998). Furthermore, estimations of the electron spectral indices inferred from microwave (δ_r) and HXR (δ_x) data during the impulsive burst phase indicate that there is a breakup in the energy spectra of the electrons (*e.g.*, Kundu *et al.*, 1994; Raulin *et al.*, 1999; Silva, Wang, and Gary, 2000). These observations may imply that two different electron populations are accelerated in different sites with distinct physical conditions. However, Trottet *et al.* (1998, 2000) found that the electron spectral index derived from observations at frequencies between 20 and 50 GHz is consistent with that inferred from γ rays. This finding confirms the view that short centimeter- and millimeter-wavelength emission come from relativistic electrons, and that these electrons may have a flatter spectrum than the electrons up to a few hundreds of keV, which dominate the HXR photon spectrum. A counter-example has been presented by White *et al.* (2003) (but see the criticism made by Klein, 2005). In any case, the TPP model may also account for the difference between δ_r and δ_x because it predicts a hardening of the spectra of the trapped electrons from the losses of lower energy electrons by energy-dependent Coulomb collisions (Trottet and Vilmer, 1984). In this case, the microwaves produced by the electrons in the trap reflect this hardening while the HXR spectra produced by the precipitated electrons preserve the original injection spectrum, which is softer.

Several studies of electron dynamics have added to the effect of Coulomb collisions on the electron energy and the effects of Coulomb collisions on electron pitch angles together with magnetic mirroring. Kundu *et al.* (1995) observed an asymmetric pair of microwave sources and interpreted it as due to asymmetric precipitation of nonthermal electrons under weak diffusion. They showed that when double HXR sources are observed the magnetically weaker footpoint is brighter in HXRs because the mirror point of the electrons is lower and more electrons precipitate there, whereas the magnetically stronger footpoint is brighter at microwave wavelengths. Asymmetric microwave sources presented in Lee, Gary, and

Shibasaki (2000) and Lee and Gary (2000) were also interpreted as due to magnetic mirroring under weak pitch-angle diffusion and the event's spectral evolution was due to not only collisional energy loss but pitch-angle diffusion.

The identification of direct precipitation in microwaves has begun relatively recently (*e.g.*, Kundu *et al.*, 2001c; Lee *et al.*, 2002). Kundu *et al.* (2001c) compared the radio time profiles of two simple spiky bursts observed with NoRH at 17 and 34 GHz with a trap model derived using the HXR 53 – 93 keV time profile. Each microwave time profile was modeled as the sum of a component identical to the HXR time profile (the injection function) and a trapped component derived by integrating over the injection function convolved with an exponential kernel function. The equation for the radio flux resulting from the trapped population alone is an integral over the trapped particle energy distribution convolved with the synchrotron emissivity. Furthermore, the microwave emission from the directly precipitating electrons will not have the same emissivity as the trapped electrons since the precipitating electrons have a different pitch-angle distribution.

The overall picture indicates that the HXR emission is dominated by footpoint sources composed of DP electrons and those that have been trapped for a time before precipitating from the loop. Although HXR emission is sensitive only to precipitating electrons, microwave emission is sensitive to the entire distribution of electrons (both trapped and DP components), but the trapped component will dominate the emission at a given frequency.

4.1.3. Anisotropies and the Effect of the Ambient Medium

The models described in Section 4.1.1 assume that gyrosynchrotron emission comes from an isotropic population of electrons in the presence of the tenuous thermal plasma. Recent studies have challenged this simplified approach: (1) The electrons may be accelerated with significant pitch-angle anisotropy or may develop it as a result of transport processes. (2) The ambient plasma may be dense enough to make plasma effects such as Razin suppression and free-free absorption, as well as high-density emission processes (*i.e.*, resonant transition radiation) important.

Evidence in favor of the pitch-angle anisotropy of microwave-producing nonthermal electrons has been reported by Lee and Gary (2000), who found clear indications of the anisotropic injection of electrons into the radio source and their consequent isotropization from angular scattering. Further evidence arises from the observation of loop-top microwave sources in optically thin bursts (*e.g.*, Kundu *et al.*, 2001b – see Figure 3 lower panel; White *et al.*, 2002). Melnikov, Shibasaki, and Reznikova (2002) found that these morphologies may arise from strong concentrations of energetic electrons at the loop top as a result of the transverse pitch-angle anisotropy of the injected electrons or may be due to enhanced loss of electrons in the lower part of the loop. The latter scenario may arise either from Coulomb collisions if in the lower parts of the loop there is higher plasma density or from an enhanced level of turbulence there. Stepanov *et al.* (2007) have argued that strong scattering of electrons by whistlers can account for the observed evolution of fast collimated ejections of nonthermal electrons reported by Yokoyama *et al.* (2002).

The idea of optically thin loop-top sources resulting from electron distributions that are strongly peaked perpendicular to the magnetic field is not consistent with models invoking DC electric field acceleration along the axes of a twisted loop or MHD turbulent cascade acceleration, in which acceleration occurs along the field lines. Although mechanisms that consider a magnetic trap collapsing after reconnection and providing conditions for betatron acceleration (Somov and Kosugi, 1997; Karlický and Kosugi, 2004) of electrons transverse to the field seem more appropriate, the energy gain from the collapse is not big and it is not clear whether it can provide the energies required by the observations.

A spectral signature of pitch-angle anisotropy has been reported from the study of bursts that have a high-frequency gyrosynchrotron component accompanied by lower frequency coherent spiky emission (Fleishman, Gary, and Nita, 2003). These microwave sources observed at angles almost parallel to the magnetic field show much softer spectra than all other events. This was interpreted as a result from the effect of loss-cone angular anisotropy on the gyrosynchrotron spectrum.

Free-free emission and absorption has been recognized as playing a role in certain flares long ago (*e.g.*, Kundu and Vlahos, 1982) as can gyroresonance absorption (Alissandrakis, Nindos, and Kundu, 1993). More recently, Bastian, Fleishman, and Gary (2007) observed an impulsive, radio-rich flare with little EUV, SXR, and HXR emissions. The radio data showed low-frequency cutoff below ~ 10 GHz and flux maxima delayed with decreasing frequency (*i.e.*, opposite to that expected for the TPP model). Furthermore, the flux decay was approximately frequency independent late in the event. They proposed that the radio emission was due to gyrosynchrotron emission from nonthermal distribution of electrons in a relatively cool, dense plasma. They suggested that energy loss by fast electrons heats the ambient plasma, reducing the free-free opacity with time, thereby accounting for the reverse delay structure.

In some cases even preflare loop densities can be significant. Veronig and Brown (2004) reported two examples of flares where the HXR emission showed that the main looplike HXR emission was located in the corona, neither at the footpoints nor above the loop top (see also Veronig *et al.*, 2005; Bone *et al.*, 2007). In these events the corona is so dense that it is collisionally thick to electrons with energies up to 50 keV, with chromospheric evaporation dominated by energy deposition through conduction rather than electron precipitation. Initial loop densities in excess of 10^{11} cm^{-3} were inferred. The concept of dense radio flares is further supported by the work of Fleishman, Nita, and Gary (2005), who found that the gyrosynchrotron emission of some 10% of all microwave bursts is accompanied by a secondary decimeter continuum component produced by the resonant transition radiation mechanism near the plasma frequency.

4.1.4. Submillimeter Emission

Submillimeter solar physics started with the advent of the Solar Submillimeter Telescope (SST; Kaufmann *et al.*, 2001) observing at 212 and 405 GHz, the Köln Observatory for Submillimeter and Millimeter Astronomy (KOSMA) observing at 230 and 345 GHz, and the Bernese Multibeam Radiometer for KOSMA (BEMRAK) at 210 GHz (Lüthi, Lüdi, and Magun, 2004; Lüthi, Magun, and Miller, 2004). Both SST and BEMRAK provide multibeam measurements that allow us to estimate the location and the averaged size of the submillimeter-emitting region.

At such high frequencies, emissions probe relativistic electrons accelerated in flares. The first observations of a flare above 200 GHz were presented by Trottet *et al.* (2002). The SST observations were combined with simultaneous OVSA observations and showed an impulsive spike produced by synchrotron emission from 10 – 15 MeV electrons and an extended phase that was mostly due to thermal free-free emission. The event studied by Lüthi, Lüdi, and Magun (2004) was not detected by HXR/γ-ray spectrometers above 300 keV. Therefore submillimeter-wavelength observations may provide a more sensitive diagnostic of relativistic electrons.

A number of submillimeter observations (Kaufmann *et al.* 2004, 2007; Lüthi, Magun, and Miller, 2004; Silva *et al.*, 2007) indicate that the radio spectrum above 200 GHz surprisingly increases with increasing frequency, in contrast to the flat or decreasing spectrum

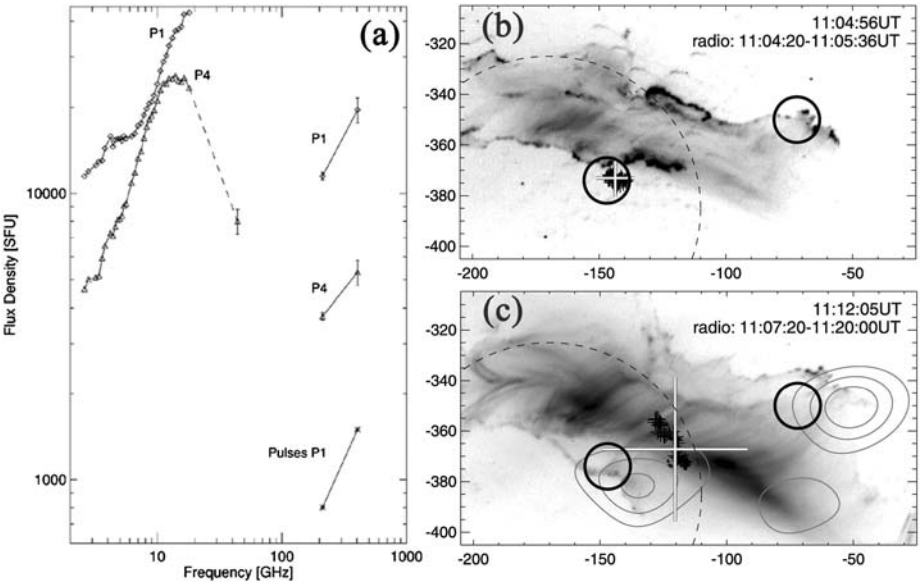

Figure 4 (a) Radio spectra of the 4 November 2003 flare. The measurements have been obtained by the OVSA between 1.2 and 18 GHz, by the Itapetinga radio telescope at 44 GHz, and by the SST at 212 and 405 GHz. (Reprinted with permission from Kaufmann *et al.* (2004).) Right panels: The 28 October 2003 flare. A TRACE image is shown for (b) 1600 Å and (c) 195 Å (with times given in the top right corner of each image) with 210-GHz centroid positions overplotted as black crosses (with a cadence of 10 s; increasing symbol size represents time). The average position and source size of the radio emission during each time interval is represented by a thick white cross. The dashed circle gives the size of the field of view of the radio imaging. The thick black circles give the flare-averaged 2.2-MeV footpoint location. The circle size represent 1σ uncertainty in the source location. The bottom image additionally shows RHESSI 250 – 450 keV imaging integrated over the decay phase. (Reprinted with permission from Trottet *et al.* (2008).)

expected for optically thin thermal free-free emission or nonthermal gyrosynchrotron emission, respectively. This is illustrated in Figure 4(a), which shows the radio spectrum observed between 2 and 400 GHz for the most intense (P1) and the less intense (P4) impulsive peaks of the 4 November 2003 flare. This event also shows fast pulses with typical durations of 0.5 s with increasing flux between 200 and 400 GHz (pulse P1 in the figure). Figure 4(a) shows clearly that the microwave emission is consistent with gyrosynchrotron emission but the submillimeter-wavelength spectral component is inverted. Note that sometimes even millimeter-wavelength observations suggest that a distinct population of high-energy electrons, separate from that producing centimeter-wavelength and HXR radiation, may be involved in the production of the millimeter-wavelength emission (*e.g.*, Kundu *et al.*, 1994). This conclusion for millimeter-wavelength emissions arises from the flattening of the electron energy distribution function toward higher energies in some flares.

The origin of submillimeter emission with increasing spectrum is not yet properly understood. Optically thick free-free emission from the flare-heated chromosphere may account for broad ($\sim 60''$) sources as the one observed by Trottet *et al.* (2008) during the extended phase of the 28 October 2003 event (Figure 4(c)). Indeed, it is compatible with a plasma at 0.2 MK whose thermal energy is only a small fraction of the total integrated irradiance of the flare. However, for compact sources like the one observed in the same flare (Figure 4(b)) and in the event studied by Kaufmann *et al.* (2004), such an interpretation is not appropriate. Indeed, although ambient temperatures of $\sim (3-4) \times 10^7$ K (*i.e.*,

in agreement with those deduced from GOES soft X-ray measurements for giant flares) are involved, emission measures that are several orders of magnitude larger than those obtained from GOES observations are also required. The possibility of producing the millimeter – submillimeter radio emission by synchrotron radiation from high-energy positrons from pions was first pointed out by Lingenfelter and Ramaty (1967). This is an attractive possibility at least for a compact submillimeter source observed in the 28 October 2003 event (see Figure 4(b)) that starts simultaneously with pion production and roughly coincides with one of the 2.2-MeV flare footpoints imaged by RHESSI (*i.e.*, with an interaction region of accelerated protons and ions). However, rough estimates indicate that the number of positrons to produce the radio emission is at least one to two orders of magnitude larger than the range of values derived from γ-ray measurements (Silva *et al.*, 2007; Trottet *et al.*, 2008). A further possibility that should be explored quantitatively is emission from proton beams as proposed by Sakai and Nagasugi (2007). Although it does not account for the temporal and spatial association with γ rays from high-energy ions, optically thin and Razin-suppressed synchrotron emission from a source different from that radiating at lower frequencies may account for the increasing flux between 200 and 400 GHz (Trottet *et al.*, 2008). For reasonable magnetic field strength (< 1000 G) and numbers of radiating electrons compatible with HXR/γ-ray measurements, the maximum of the high-frequency spectrum can hardly exceed 400 GHz.

4.2. Late-Phase Emissions

In the decay phase, optically thin thermal free-free emission is the dominant but not exclusive mechanism at microwaves. This shows well in long-duration events (LDEs): Usually nonthermal gyrosynchrotron emission as well as HXRs are observed only in their rise phase, whereas later on the microwave observations show the brightening of arcade loops resulting from free-free emission from the hot, dense plasma (see Hanaoka, 1999, for a review). Occasionally, nonthermal signatures in the late phase of microwave and millimeter-wavelength flares have been reported (*e.g.*, Alissandrakis, Schadee, and Kundu, 1988; Kundu *et al.*, 2004; Trottet *et al.*, 2008). LDEs are considered eruptive flares and have a strong link to CMEs. However, Altyntsev *et al.* (1999) and Grechnev, Kundu, and Nindos (2006) have reported LDEs originating from interacting closed loops. Furthermore, Goff *et al.* (2007) analyzed an event that consisted of three flares and a CME. The first two flares were impulsive confined flares but the third was an LDE. Contrary to the usual paradigm, the two first flares were linked to the CME onset, whereas the third flare was only related to the relaxation of the coronal magnetic field after the CME had left the corona.

At metric and decimetric wavelengths, long-lasting broadband quasi-continuum features (type IV bursts) often appear in the decay phase of strong flares. These bursts often present significant fine structure (see Section 5). Type IVs have previously been interpreted by loss – cone emission of trapped electrons. However, their spectral fine structure and its weak correlation with HXR subpeaks (Benz *et al.*, 2005) as well as their preferential *o*-mode polarization may imply that type IVs are due to a coherent plasma process. However, the faint and smooth continua associated frequently with the release of CMEs (Aurass *et al.*, 1999) are due to synchrotron radiation (Bastian *et al.*, 2001). Type IVs at meter wavelengths are usually seen with type II radio bursts.

Type IV bursts are not directly related to the primary energy release and acceleration process. Their association with LDEs has led to the idea that a portion of the long gradual energy release occurring in the LDE arcade accelerates electrons that then produce type IV emission on closed field lines in the arcade (Lantos *et al.*, 1981; Kahler and Hundhausen,

1992). Therefore type IV bursts are linked to energy release and reconfiguration of the coronal magnetic field that are distinct from those responsible for the main phase of the flare. This interpretation is supported by the association of type IV emission with interplanetary electrons (*e.g.*, Klein *et al.*, 2005).

5. Electron Acceleration Episodes Associated with Radio Fine Structure

Sporadic solar radio emission shows an extraordinary variety of structure in frequency and/or time, some of which is beyond or at the limit of our present observing facilities. Here we confine our discussion to those fine structures that are not intrinsic parts of bursts of type I (see Section 3.2.2), type II (herringbone structures; see Section 7.1), and type III (groups of type IIIs; see Section 3.1) and have something to tell us about electron acceleration. (For a detailed review, see Nindos and Aurass (2007).)

5.1. Narrowband Spikes

Individual spikes are very short (< 1 s), narrowband (some MHz only) bright emissions forming broadband clusters or patches of some tens to thousands during some tens of seconds to about a few minutes (see Benz, 1986, for a review). Clusters are sometimes organized in small subgroups or chains. The spike's bandwidth constrains its source size. By assuming that the emission frequency depends on a characteristic frequency (*e.g.*, the local plasma frequency or a harmonic of the gyrofrequency) an upper limit of spike's source dimension L can be given by the product of the scale length of the characteristic frequency multiplied by $\Delta f/f$. Using typical values, Benz (1986) found that $L \leq 200$ km.

It is debated whether or not narrowband decimetric spikes are signatures of accelerated particles at the primary energy release site. A popular idea is that they represent a signature of highly fragmented energy release in flares (Benz, 1985). Theoretical models that propose that the spikes come from sources located in the acceleration site of the flare have been developed (*e.g.*, Kuijpers, van der Post, and Slottje, 1981; Tajima *et al.*, 1990; Stepanov *et al.*, 1999). More recently, Bárta and Karlický (2001, 2005) have developed a model (see also Section 5.2) in which decimeter spikes can be generated in the turbulent plasma of reconnection outflows. They find that at these turbulent regions either decimeter spikes or other more rare fine structures should be observed depending on the turbulence's properties.

The hypothesis that narrowband metric spikes are closely related to the acceleration region of electron beams that escape to the high corona is supported by the work of Benz *et al.* (1982), who found that in 10% of all groups of metric type III, narrowband metric spikes are found slightly above the start frequency of the type IIIs and small clusters of metric spikes show temporal correlation with individual type IIIs and thus with the acceleration of electron beams. This result is consistent with the more recent one by Paesold *et al.* (2001), who have found double type III sources to diverge from the same spike source.

Other approaches have also been pursued. Fleishman and Melnikov (1998) propose that the spike properties can be interpreted in terms of electron cyclotron maser (ECM) emission produced by energetic electrons ($E \sim 10-100$ keV) with a loss-cone pitch-angle distribution. They suggest that the source of a spike cluster is a loop with local inhomogeneities forming traps, where the pitch-angle anisotropy is stronger than on average and provides strong local wave amplification as a result of negative gyrosynchrotron absorption. Thus, each local trap forms a site where a single spike is generated. Some observational support for their model is provided by the analysis presented by Fleishman, Gary, and Nita (2003).

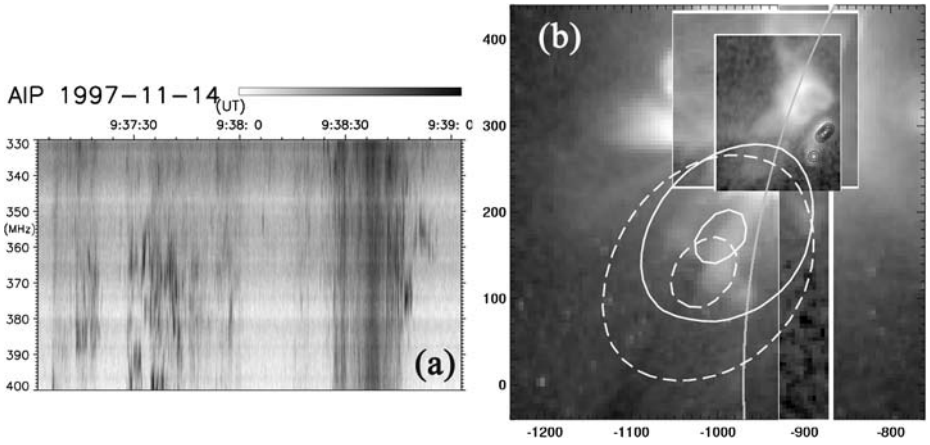

Figure 5 (a) An Astrophysikalisches Institut Potsdam (AIP) spectrogram showing spike clouds. (b) The gray-scale image is a composite of full-frame and partial frame *Yohkoh* SXT images. The black contours denote the HXR image; white contours show the location of spike bursts presented in the left panel according to NRH maps (with the dashed and solid contours showing the 60% and 90% contour levels for the NRH 327- and 410-MHz sources, respectively, at 09:38:30 UT). The SXR looplike feature northeast of the HXR contours is related to the CME-associated flare (from Khan and Aurass, 2006; reprinted with permission).

Furthermore, the finding by Aschwanden and Güdel (1992) that the integrated spike flux is delayed by 2 – 5 s with respect to the associated HXR peaks is also inconsistent with the interpretation of the spikes as tracers of the primary energy release.

Khan and Aurass (2006) found one case where narrowband radio spike bursts are seen as a side phenomenon just during the liftoff of a structure related with a CME. Figure 5 shows a composed overlay of *Yohkoh* SXT and HXT images with isolines of the spike cloud emission at 327 and 410 MHz from simultaneous NRH data. Their analysis reveals that the eruption pushes the surrounding magnetic structures southward where they come into contact with neighboring magnetic loops. During this large-scale loop collision, the spikes occur far away from the associated HXR sources, even though some correlation between smoothed HXR- and frequency-integrated radio flux curves was found. These results confirm earlier observations by Benz, Saint-Hilaire, and Vilmer (2002), who reported spike clusters located well outside the main energy release region of a flare.

5.2. Broadband Decimetric Fine Structures

Decimetric pulsations are broadband emissions ($\Delta f/f \sim 0.5$) with periodic or irregular short fluctuations. Sometimes they are quasi-periodic with pulses of 0.1 to 1 s separations, occurring in groups of some tens to hundreds and lasting a few seconds to minutes. Some decimetric events occur in continuum patches with drifting upper and lower frequency boundaries, with the drift being predominantly directed toward lower frequencies. Such patches are called drifting pulsating structures (DPS). DPS have been found to be associated with the impulsive phase of flares, although they can occur before or after the HXR burst peak and can be associated with plasmoid ejections seen in soft X-rays or EUV (*e.g.*, Wang *et al.*, 2001; Kundu *et al.*, 2001a; Karlický, 2004; Karlický, Fárník, and Mészárosová, 2002; Khan *et al.*, 2002; Kolomanski *et al.*, 2007).

DPS have been interpreted in the framework of a model in which the radio pulsations are caused by quasi-periodic particle acceleration episodes that result from magnetic reconnec-

tion in a large-scale current sheet (Kliem, Karlický, and Benz, 2000). Under these circumstances, a possible reconnection model is the one in which reconnection is dominated by repeated formation and subsequent coalescence of magnetic islands. This process is known as secondary tearing or as an impulsive bursty regime of reconnection. The continuously growing plasmoid is fed by newly coalescing islands. The plasmoid becomes strongly accelerated along the sheet and the pulsating particle source is located at the magnetic X-line adjacent to the plasmoid. The radio source is then formed in or near the plasmoid. The frequency drift of the pulsating structures can naturally be attributed to the rise of the plasmoid in the corona or to the growing upward expansion of the current sheet. Using MHD and PIC simulations Karlický and Bárta in a series of papers (*e.g.*, Karlický, 2004; Bárta and Karlický, 2005; Karlický and Bárta, 2007) have refined this scenario and have shown that the interpretation of DPS in terms of electron beams injected into plasmoids can reproduce several of their observed features.

5.3. Zebra Patterns and Fiber Bursts

In dynamic spectra zebra patterns consist of intermittent bright and dark stripes superimposed on the background continuum. They were first discovered at metric wavelengths several decades ago but later they have been observed at decimetric and microwave wavelength ranges as well (*e.g.*, Elgarøy, 1959; Aurass *et al.*, 2003; Zlotnik *et al.*, 2003; Chernov, Yan, and Fu, 2003; Chernov *et al.*, 2006; Altyntsev *et al.*, 2005). The existing models of zebra patterns can be divided into the following classes: (1) models based on the double plasma resonance and subsequent transformation of generated plasma (upper hybrid in fact) waves into the electromagnetic mode (Zheleznyakov and Zlotnik, 1975; Zlotnik *et al.*, 2003; Ledenev, Yan, and Fu, 2001); (2) models involving the nonlinear coupling of Bernstein modes (Altyntsev *et al.*, 2005, and references therein); and (3) the model based on the eigenmodes of plasma waves trapped in a resonator-like structure formed by local plasma inhomogeneity (LaBelle *et al.*, 2003). Alternatively Bárta and Karlický (2006) propose that zebra patterns may be considered an example of a pattern possibly caused by phase-coherent effects.

Fiber bursts appear in some complex solar radio bursts as narrow fine structure that drifts in frequency with time within broadband emission in the metric- and decimeter-wavelength range. A model (proposed by Kuijpers, 1975, modified by Mann and Motschmann, 1987; Mann *et al.*, 1989, and recently confirmed by Rausche *et al.*, 2007) for these bursts invokes whistler waves ascending postflare coronal loops, which also act as magnetic traps for nonthermal flare electrons. The whistler frequency can be derived from the pattern of emission ridges and absorption channels in the dynamic spectrum: Adjacent emission ridges are assumed to be separated by the whistler frequency. Since the emission mechanism is believed to be plasma emission, the ambient electron density is simply determined from f_p. Knowing the whistler frequency then allows the magnetic field to be determined. Aurass *et al.* (2005) compared the resulting fields at locations known from radio imaging data with magnetic field strengths determined from an extrapolation of surface fields and found good consistency between the two methods by fitting the parameters of a Newkirk-like local density model. Note that an alternative approach has been followed by Bernold and Treumann (1983) and Treumann, Güdel, and Benz (1990), who invoked Alfvén solitons to explain fiber bursts (but their model seems not to be appropriate for the events analyzed by Aurass *et al.*, 2005, and Rausche *et al.*, 2007).

In many cases, both zebra patterns and fiber bursts, as well as metric broadband pulsations, occur within type IV bursts. For one particular event, a unified source model for all of these structures has been outlined by Zlotnik *et al.* (2003).

6. Radio Emission from Large-Scale Eruptions

In this section, we discuss radio emission associated with CMEs as well as radio emission from prominence eruptions. Features that sometimes are used as CME proxies (shocks and coronal waves) might not be related to CMEs but rather to cotemporal flares; these phenomena are discussed in Section 7.

6.1. CME Detection

Plasma emission is the most usual radio emission associated with CME, including type II (see Section 7) and IV and IVm solar bursts. Moving type IVs (IVm) are outward-moving radio blobs associated with CMEs. They occur rarely and include isolated plasmoids (Wagner *et al.*, 1981), expanding arches, and advancing fronts (Stewart, 1985). We note that plasma emission is not the only possible emission mechanism for IVm bursts. An alternative explanation is gyrosynchrotron emission. The morphology of plasma-emission-associated sources may be different from the white-light CME because plasma emission arises near the plasma level or its second harmonic; therefore care should be exercised in the comparison between such radio sources and coronagraphic data.

The material carried away by CMEs is expected to produce optically thin free-free emission. Ideally, it is anticipated that the free-free emitting structures will look similar to the structures seen by the coronagraphs because both correspond to multithermal plasmas and depend on the emission measure (radio) and column density (white light) of the electrons. However, since coronal temperatures and low densities dominate CMEs, their free-free emission is expected to be weak and often masked by bright nonthermal emissions. Only a few observations of thermal free-free emission from CMEs have been reported at low frequencies. Early observations were obtained at frequencies below 80 MHz, which are not accessible with today's imaging instrumentation (*e.g.*, Sheridan *et al.*, 1978; Gopalswamy and Kundu, 1992). More recently, Maia *et al.* (2000) have imaged CME fronts with the NRH at frequencies between 450 and 164 MHz. The sources moved at speeds consistent with white-light CME fronts and their brightness temperature was a few 10^4 K, implying thermal origin. However, their polarization and spectral behavior challenged the thermal interpretation. Detection of thermal emission from CMEs has been reported by Kathiravan, Ramesh, and Subramanian (2002) and Ramesh *et al.* (2003), who used the Gauribidanur Radioheliograph at 109 MHz. When the thermal nature of the emission is established, the computation of the mass contained in the CME is straightforward. Masses obtained from radio observations are similar to those of white-light CMEs (Gopalswamy and Kundu, 1992).

Gyrosynchrotron emission from even a small number of nonthermal electrons, entrained in the CME magnetic field, can easily exceed the thermal emission by a few orders of magnitude. The brighter gyrosynchrotron signal will correspond to the locations of the strongest magnetic field within the CME. CME loop systems illuminated by gyrosynchrotron emission have been detected by Bastian *et al.* (2001) and Maia *et al.* (2007) using the NRH. The properties of both events were similar and here the 410-MHz images by Maia *et al.* (2007) are given in Figure 6. They show the radio CME clearly; its speed was found to match the speed of the white-light CME. Plasma radiation cannot account for the observed properties of the radio emission because (1) the source emitted at a fixed frequency over a spatial extent of more than $1\,R_\odot$ (see Figure 6), which would require a uniform electron density throughout the source, and (2) the radio loops were cospatial at all five observing frequencies; if the emission came from plasma radiation, spatial dispersion in the source location as a function of frequency would be observed.

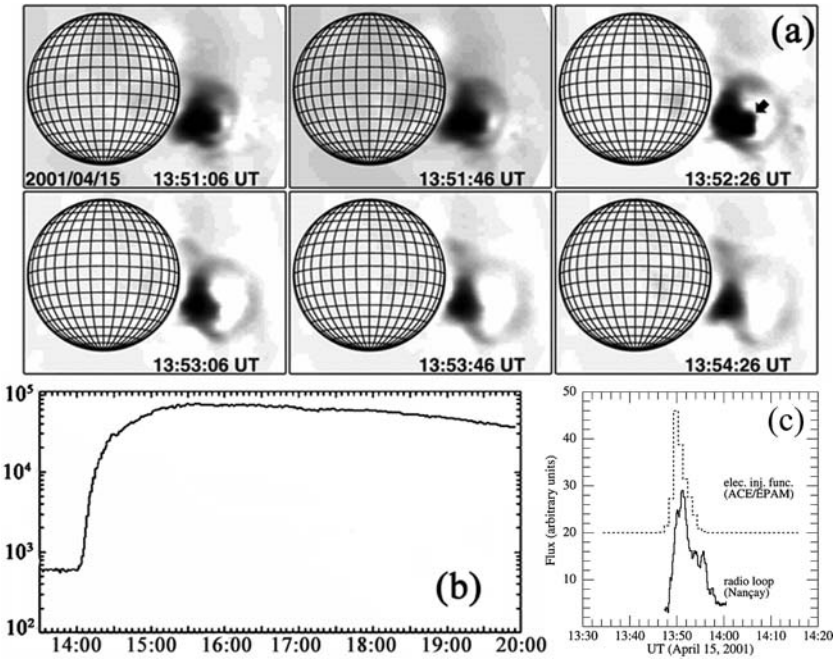

Figure 6 (a) Series of NRH 410-MHz images showing the progression of a radio CME on 15 April 2001. (b) Plot of 1-minute-integrated 178 – 290 keV electron flux as seen by the EPAM experiment on the ACE spacecraft. (c) Comparison of the derived near-relativistic electron injection function (dashed line) and radio loop flux at 432 MHz (solid line). (Reprinted with permission from Maia *et al.* (2007).)

The detection of gyrosynchrotron loops at several frequencies enables the calculation of the spectral indices along the loops. In the events studied by Bastian *et al.* (2001) and Maia *et al.* (2007) the radio spectrum shows evidence for suppression from the Razin effect. By fitting the observed spectra with model synchrotron spectra, the energy of the nonthermal electrons, the magnetic field, and the density of the thermal electrons can be determined. The two studies yielded energies of about 0.5 – 10 MeV, magnetic fields of $\sim 0.1 - 10$ G, and thermal densities of $\sim 10^7$ cm^{-3}.

Concerning the origin of the energetic electrons responsible for the gyrosynchrotron CME loops, Bastian *et al.* (2001) suggest three possible sources: (1) They are injected into the large-scale coronal loops by associated flare activity relatively low in the corona; (2) they are accelerated in a reconnecting current sheet in the aftermath of the CME launch; or (3) they are accelerated by the CME-associated shock.

6.2. CME Development

The unprecedented cadence (< 1 s) and large field of view (at meter wavelengths) on the disk and above the limb of radio imaging data make them ideal to study the development of CMEs from their early stages. In all events that have been studied the radio emission revealed multiple loops participating in the eruption process whose development was faster than the cadence of the EIT or LASCO instruments. The first LASCO-radio-imaging observations of the development of a CME were reported by Maia *et al.* (1998). A limb CME was observed and the radio images allowed the identification of successive loop interactions from the site

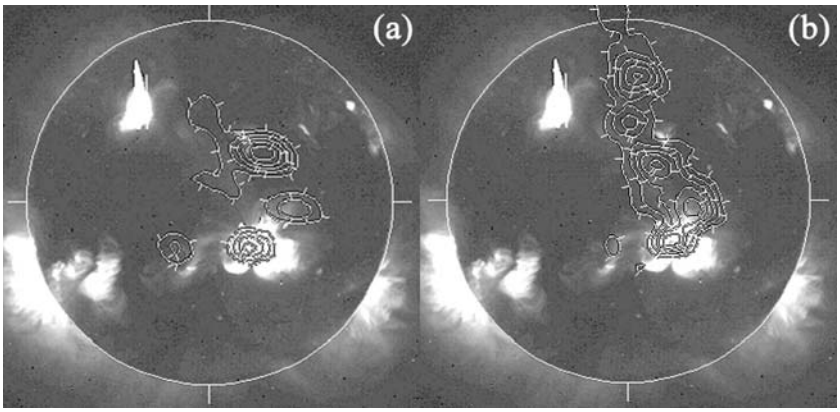

Figure 7 (a) NRH 236-MHz sources at 13:39:13 UT (contours) plotted over the *Yohkoh* SXT image at 13:26:59 UT on 2 May 1998. (b) Nançay 327-MHz sources at 13:39:57 UT (contours) plotted over the same *Yohkoh* image. (Reprinted with permission from Pohjolainen *et al.* (2001).)

of the associated flare to larger and larger distances, leading to radio sources with latitudinal extent similar to the white-light CME. A similar analysis was performed by Pohjolainen *et al.* (2001). They studied a halo CME associated with a major flare from AR8210 (located at the southwest part of the solar disk in the images of Figure 7). The SXR images show a set of transequatorial loops that connect AR8210 with smaller ARs north and northeast of it whereas shorter and brighter loops connect it with a bipolar region east of it. In the early phase of the flare, radio sources traced the propagation paths of energetic electrons roughly along these loops but in the main phase of the flare, new radio sources (see Figure 7) appeared, presenting signatures of destabilization and reconnection at discrete locations of the connecting loops. The subsequent disappearance of the connecting loops led Pohjolainen *et al.* (2001) to interpret these radio sources as possible signatures of the CME liftoff on the disk. The opening of the magnetic field associated with the CME was revealed by an expanding moving radio source overlying the EIT dimming region. Furthermore, Klein *et al.* (2001) have reported that, in one large event, moving radio sources ascribed to magnetically confined populations of nonthermal electrons could reveal reconnection far from the flaring active region.

Radio observations combined with observations at other wavelength ranges and magnetic field extrapolations can help us check CME initiation models against observations. Marqué, Lantos, and Delaboudinière (2002) combined EUV and radio imaging observations of coronal plasma structures including a quiescent filament with coronographic observations of a CME to infer the origin of the eruption on the disk. The radio images show that an underdense structure, presumably the filament cavity, became unstable. Its time – height diagram continued smoothly into the CME seen later by the coronagraph. The configuration was consistent with flux rope models of filaments (Low and Hundhausen, 1995).

The studies by Maia *et al.* (2003) and Manoharan and Kundu (2003) are based on nonthermal radio emission. Maia *et al.* (2003) studied a complex event in which radio observations revealed multiple loop systems at distant locations that became active and participated in the eruption. The magnetic field extrapolations revealed the presence of a coronal null point in the vicinity of the CME-associated flare. Its presence combined with the occurrence of two distant and nearly simultaneous radio sources favors the generalized breakout model for the triggering of the eruption (Antiochos, DeVore, and Klimchuk, 1999;

Aulanier *et al.*, 2000). We note, however, that the altitude of the null point was too low for its activity to be detectable at the NRH frequencies. Manoharan and Kundu (2003) derived similar results. Furthermore, Aurass, Rausche, and Mann (2007) detected a continuum meter- to decimeter-wavelength source from magnetic field converging separatrices, and Pohjolainen *et al.* (2005) used NRH images that helped them determine the time and location of a CME-associated large-scale field line opening; the radio sources traced the electron propagation paths above the active region and along the transequatorial loop system, in which large-scale mass depletion later took place. Large-scale field line opening preceding the liftoff of material is an essential part of the breakout model. Aurass *et al.* (1999) have reported that faint drifting continua might indicate the opening of coronal structures just before the CME's onset.

6.3. Prominence Eruptions

Radio observations complement Hα prominence observations: The Hα emission depends critically on the plasma temperature but because prominences contain cool (~ 8000 K) and dense ($\sim 10^{10} - 10^{11}$ cm^{-3}) material they radiate optically thick thermal free-free emission at microwaves (*e.g.*, Gopalswamy and Hanaoka, 1998), which can be imaged with clarity outside the disk. (Note, however, that quiescent filaments, *i.e.* prominences when seen on the disk, appear as brightness depressions at microwaves.) The spatial resolution of microwave images is not as high as that of Hα images but since the free-free radiation is a continuum emission the prominence can be observed even when it is heated to a higher temperature whereas heated prominences may disappear in Hα. The radio data provide estimates of the prominence mass (*e.g.*, Gopalswamy and Hanaoka, 1998) but such calculations do not take into account possible downflows of material as the prominence rises.

Several case studies of prominence eruptions at microwaves (see Figure 8 for an example) have been reported (*e.g.*, Hanaoka *et al.*, 1994; Gopalswamy *et al.*, 1996, 1999; Hori, 2000; Uralov *et al.*, 2002; Grechnev *et al.*, 2006). These studies show that the radio data provide information about the early phase of the CME that is not accessible by using coronagraphic data only; in most of them the eruptive prominence observed in the radio field of view eventually becomes the core of the associated white-light CME. This is demonstrated in the height – time plot of Figure 8, where the diamonds denote prominence height measured from the radio data and the squares denote the height of the prominence core measured from the LASCO images. The high degree of association between microwave prominence eruptions and CMEs has been confirmed by the statistical studies by Hori and Culhane (2002) and Gopalswamy *et al.* (2003).

Hudson *et al.* (2001) have reported a moving HXR source associated with an erupting prominence. The event has been imaged by NoRH at 17 GHz and, according to Gopalswamy (2006a), part of the microwave emission is of nonthermal origin.

7. Radio Emission from Shocks

7.1. Coronal Type II Bursts

Coronal type II bursts (see Figure 9 for an example) typically occur at around the time of the SXR peak in a flare and often appear as two bands with a frequency ratio of about 2 in the range $\sim 20 - 400$ MHz that drift slowly downward in frequency. Under the assumption that the exciter propagates along the gradient of a typical coronal density model the drift rate

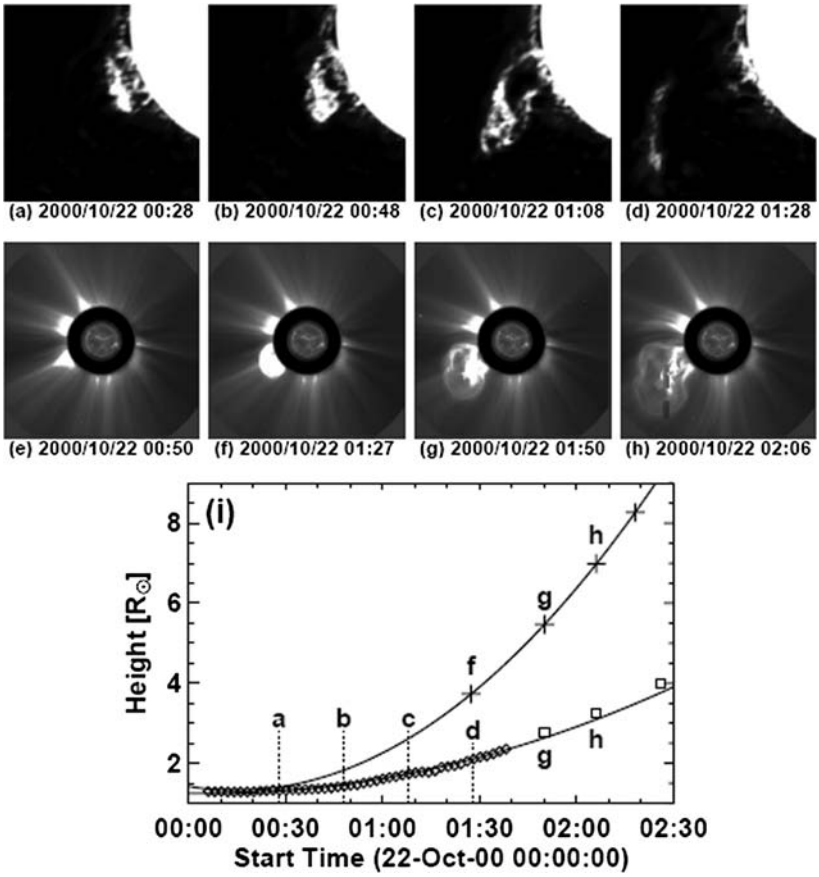

Figure 8 (a) – (d) NoRH 17-GHz images of a prominence eruption. (e) – (h) LASCO images of the white-light CME that eventually develops the typical three-part structure. (i) The height – time plots of the CME (upper curve) and the eruptive prominence (lower curve). The diamonds and squares denote heights of the prominence measured from the NoRH images and heights of the CME core, respectively. The curves resulted from fitting second-order polynomials to the data points. (Reprinted with permission from Gopalswamy *et al.* (2003).)

yields speeds of 500 – 1000 km s^{-1}, whereas the Alfvén speed in the low corona is thought to be typically several hundred kilometers per second; this led to the idea that type II bursts are generated by MHD shocks traveling at several times the local Alfvén speed. The shock moves through the corona and radio emission is produced at the plasma frequency and its harmonic by nonlinear processes involving Langmuir waves, which are driven by electron beams accelerated at the shock (*e.g.*, Nelson and Melrose, 1985; Mann, Classen, and Aurass, 1995).

Each type II band can be further split into upper and lower bands thought to be caused by the density jump in the shock (*e.g.*, Nelson and Melrose, 1985; Mann, Classen, and Aurass, 1995; Vršnak *et al.*, 2001). Consequently, one can use the split to evaluate the density jump at the shock front and estimate the shock Mach number. Measuring the frequency gap between the split bands, Vršnak *et al.* (2001) inferred that the density compression ratios range from 1.1 to 2.6 across coronal type II shocks, corresponding to Alfvénic Mach numbers of

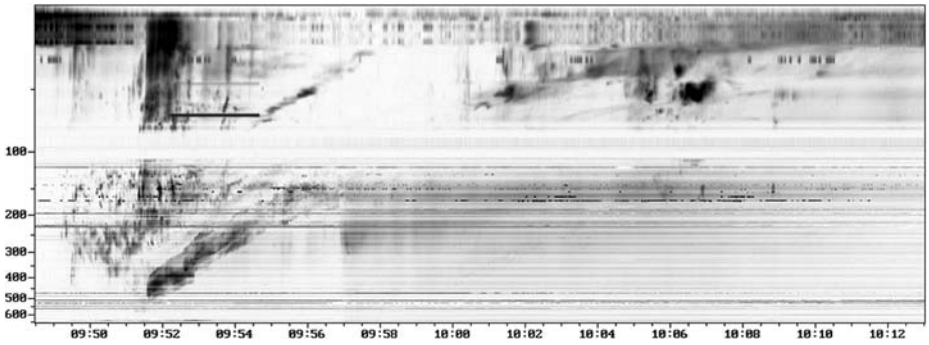

Figure 9 Dynamic spectrum of the 3 November 2003 event obtained by Artemis (from Alissandrakis *et al.*, 2005).

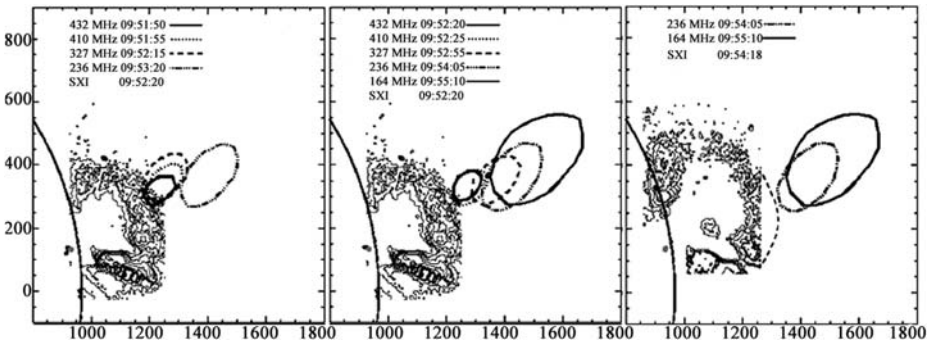

Figure 10 Contours (taken at 70% of the maximum) of the type II emissions at different NRH frequencies for the event presented in Figure 9, together with the contours of the GOES/SXI difference images taken, respectively, at 09:52:20 and 09:54:18 UT. The dashed curve in the latest image shows the extrapolation of the GOES/SXI loop outside of the GOES/SXI field of view (from Dauphin, Vilmer, and Krucker, 2006; reprinted with permission).

around 2 (see also Cho *et al.*, 2007). Note that from a completely different diagnostic (*i.e.*, UV spectroscopy of a shock in front of a LASCO CME), Raymond *et al.* (2000) found similar compression ratios.

Sometimes the main signature of a type II burst, called "backbone," is accompanied by rapidly drifting stripes of radio emission emanating from the "backbone" toward both high and low frequencies. These "herringbones" are regarded as signatures of upstream and downstream electron beams, which are accelerated by the shock waves associated with the backbone. Their drift rates yield speeds of about $0.1c$, which correspond to energies of a few keV (*e.g.*, Mann and Klassen, 2002).

7.1.1. The Origin of Coronal Type II Shocks

The launch of coronal shocks requires a sudden disturbance to be introduced in the corona that will propagate faster than the local Alfvén speed. In terms of their generation mechanism, coronal shocks can be classified into blast shocks and driven shocks. In the former class the initial perturbation has the form of a large-amplitude disturbance of the medium,

which propagates as a nonlinear simple wave (Mann, 1995). The perturbation profile steepens until a shock is generated (*e.g.*, Vršnak and Lulic, 2000). As it propagates its amplitude drops because of geometrical expansion, dissipation, and the widening of the perturbation profile and ultimately it decays to a small-amplitude wave. In contrast to blast shocks, driven shocks are constantly supplied with energy by a driver or piston. The origin of blast waves in the corona is generally ascribed to explosive energy conversion in flares, whereas driven shocks are attributed to CMEs, with the more or less explicit idea that the type II emission comes from their bow shock.

Statistical studies show that metric type II bursts occur during events where both flares and CMEs are observed. Several authors tried to establish a classification in terms of association with either of these phenomena (*e.g.*, Classen and Aurass, 2002; Shanmugaraju *et al.*, 2006). The majority of "flare-associated" type II bursts (*i.e.*, type II bursts that lack a clear CME association) occurs with flares within 30° from central meridian, where CMEs are more difficult to observe. Thus the statistical identification of type II bursts without CME may rely on an observational bias that STEREO will remove. Metric type II bursts without a minor or a major CME seem to be exceptional cases, if they exist. However, whenever a metric type II is observed without a flare, there are good reasons to believe that the flare occurred behind the solar limb.

Few comparisons between type II burst imaging and white-light CMEs have been reported because the heights that correspond to the radio frequency range accessible from the ground are occulted in space-borne coronagraphs. When simultaneous images are available, the type II burst usually appears lower than the CME front (*e.g.*, Gary *et al.*, 1984; Klein *et al.*, 1999b) even though a few cases where the shock source is located at or near the CME front have been also reported (*e.g.*, Robinson, 1985; Maia *et al.*, 2000). Wagner and MacQueen (1983) discuss early evidence on the different locations of the CME front and metric type II sources. But the comparison is difficult to make because electron acceleration at shocks may be restricted to quasi-perpendicular regions so that some difference between spatially restricted sources of type II emission and the white-light CME are to be expected (Steinolfson, 1985). Stewart (1984) and Mancuso and Raymond (2004) suggest that the apparent lag between CME leading edge and the type II source could be a geometrical effect. They note that shock strength will be enhanced along streamer axes (because of their lower Alfvén speeds) and that such streamers are characteristically offset from the axis of symmetry along which the CME propagates. The presumably low magnetosonic Mach number of traveling disturbances in the corona could indeed explain why a given disturbance creates shocks only in specific structures with low Alfvén speed.

These results suggest that metric type II bursts are not emitted by the bow shocks of CMEs. Maia *et al.* (2000), however, identify faint metric radio emissions with drift rates similar to the ones observed in type II bursts, which came from elongated sources near the backward extrapolation of the CME front later seen by the coronagraph. Since a usual type II burst was observed earlier during the same event, it is likely that the two phenomena were independent: The bow shocks of fast CMEs may indeed generate type-II-like emission at meter wavelengths, but it is too weak to be clearly identified as such in dynamic spectrograms. The usual metric type II burst is probably not emitted at the bow shock of a CME – a conclusion that corroborates the suggestion of Wagner and MacQueen (1983).

This does not imply that metric type II shocks are pure blast waves. Green *et al.* (2002) discuss a major flare (GOES X class) near the limb without fast conspicuous mass motions and no type II emission. This may suggest that even a large event of explosive energy conversion is not sufficient for a type II burst to occur if there is no rapid macroscopic mass motion (*i.e.*, no magnetic piston). There are also other problems regarding the blast shock

interpretation. (1) Cliver, Webb, and Howard (1999) emphasize the lack of correlation between flare size and type II occurrence: Many type IIs are associated with relatively weak flares, which nonetheless have fast CMEs. (2) When examining the relative timing between type IIs and CMEs one should take into account the variation of the Alfvén speed in the corona (Warmuth and Mann, 2005): The usual appearance of type IIs after the flare's impulsive phase may be because the CME driver does not reach super-Alfvénic speeds early on.

White-light CMEs are not the only possible driver of coronal shock waves. Small scale ejecta (*e.g.*, sprays, soft X-ray jets and plasmoids, and erupting loops) can also ignite coronal shocks. Evidence for the generation of metric type II bursts by expanding SXR features have been reported by Gopalswamy *et al.* (1998, 2001b), Klein *et al.* (1999b), Klassen, Pohjolainen, and Klein (2003), and Dauphin, Vilmer, and Krucker (2006). These structures act as temporary pistons, generating an initially driven shock. After the expansion stops, the disturbance travels as a blast shock. An example of such an event is shown in Figure 10. Radio sources at different frequencies are found above an expanding soft X-ray loop. The scenario is consistent with type II emission from the bow shock of this loop.

A clear connection of some metric type II bursts with flare-related energy release is shown by type II "precursor" emission, whose properties were first identified by Klassen *et al.* (1999). These are bursts of different spectral types (such as type III pulsations) that occur before a type II burst, and whose high- and/or low-frequency cutoffs are consistent with the backward extrapolation of the drifting type II bands. The precursors occur together with HXR or microwave emission. Their source region lies between the region of SXR emission of the flare and the region where the subsequent type II burst starts. This is a further illustration of the close association of the various phenomena of explosive energy conversion in flare – CME events; it has been shown (Zhang *et al.*, 2001) that CMEs may accelerate impulsively in conjunction with the flare impulsive phase (see also Veronig *et al.*, 2006; Vršnak *et al.*, 2006; Temmer *et al.*, 2007, for more recent case studies).

7.1.2. Relation to Other Coronal Wave Phenomena

The close temporal and spatial association between Moreton waves and type II bursts (*e.g.*, Kai, 1970; Khan and Aurass, 2002; Pohjolainen *et al.*, 2001; Warmuth *et al.*, 2004) has been used as evidence for the flare origin of most type IIs because traditionally Moreton waves are considered as the "ground track" of flare-produced coronal MHD wavefronts that sweep over the chromosphere (Uchida, 1968). Uchida, Altschuler, and Newkirk (1973) calculations predict the refraction of the shock wave into regions of low Alfvén speed. This feature of Uchida's theory is supported by several imaging observations (*e.g.*, Nelson and Robinson, 1975) of type IIs that show that the alignment of type II source positions at successively lower frequencies deviates significantly from radial with respect to the associated flare. However, alternative explanations have been also used: preferential acceleration of electrons in restricted regions of the shock front (*e.g.*, the quasi-perpendicular regime; Steinolfson, 1984) or suitable orientation of the motion of the shock driver as well as the magnetic environment where the type II occurs (Aurass, Hofmann, and Urbarz, 1998; Klein *et al.*, 1999b). A summary of coronal wave phenomena is given by Warmuth (2007).

Type IIs show a close relationship with EIT waves (*e.g.*, Mann *et al.*, 1999; Klassen *et al.*, 2000) even though the deduced propagation velocities may differ significantly. (Usually the velocity discrepancies are interpreted in terms of the low EIT cadence and the possibility of oblique motion of the type II source with respect to the radial direction.) However, the reverse is not true: Biesecker *et al.* (2002) report that only 21% of EIT

waves are accompanied by type IIs. We note that alternative interpretations that challenge the wave nature of "EIT waves" have been developed (*e.g.*, Delannée and Aulanier, 1999; Attrill *et al.*, 2007). If only the fastest of the propagating disturbances called "EIT waves" were MHD shock waves, as suggested by Warmuth (2007), the poor association with type II shocks found by Biesecker *et al.* (2002) would become consistent with the other statistical studies.

7.2. Interplanetary Type II Bursts and Their Relation to Coronal Type II Bursts

There is a large body of work on IP type II bursts, at frequencies from 20 MHz to ~ 20 kHz, which can be seen out to 1 AU. We limit the following discussion to a few features that can help us understand coronal type II bursts, rather than attempting an exhaustive review of the radio emission from IP shocks.

Type-II-emitting shocks that have been studied by *in situ* measurements were found to be quasi-perpendicular and to be observed before the arrival of interplanetary CMEs (Bale *et al.*, 1999; Hoang *et al.*, 2007). Unlike coronal type II shocks, the IP type II shocks are therefore generally considered to be the bow shocks of CMEs.

It is well established from observations that metric type II bursts (1) are much more frequent than IP type II bursts and (2) do not generally extend to hectometric wavelengths (*e.g.*, Gopalswamy *et al.*, 1998; Cane and Erickson, 2005). Most metric type II bursts appear to die out within heliocentric distances of $\sim 2R_{\odot}$ since they are rarely observed to extend below 5 MHz. This suggests that they are driven by shock waves that die out within a few solar radii above the photosphere. However, in some cases, the shock motion can be well traced from the Sun to the Earth orbit (*e.g.*, Leblanc *et al.*, 2001) but in others two independent shocks (a coronal shock and an IP one) are invoked for the interpretation of the observations (*e.g.*, Reiner *et al.*, 2001).

A possible reason for the distinction of coronal and IP type II bursts may be the variation of the Alfvén speed with the distance from the Sun (Mann *et al.*, 2003; see also Gopalswamy *et al.*, 2001a; Warmuth and Mann, 2005). The models suggest that the Alfvén speed has a maximum of around 800 km s^{-1} at a heliocentric distance of a few solar radii. This height may separate coronal from IP type II bursts, since a given disturbance has a better chance of steepening into a shock inside or outside of this heliocentric distance, whereas few disturbances will be able to generate a shock all the way (Gopalswamy, 2006b). Emission from the nose and flanks of the same shock might explain the occasional events with simultaneous bands of emission in the metric and IP domains (Raymond *et al.*, 2000). The different slopes of the curve of the Alfvén speed as a function of the distance from the Sun below and above the local Alfvén speed peak may explain why the drift rates of coronal and IP type II bursts are different. However, these arguments do not exclude rigorously the possibility that in several events two shocks are at work (*e.g.*, Cane and Erickson, 2005).

7.3. Electron Acceleration at Coronal Shocks

7.3.1. Efficiency of Shock Acceleration

Owing to the coherent nature of plasma emission one cannot derive the number and energy of the electrons accelerated at coronal shocks directly from the spectrum of type II bursts. The efficiency of electron acceleration by coronal shocks can be evaluated more reliably by using simultaneous HXR observations. Klein *et al.* (2003) analyzed an event from an occulted AR and found that the upper limit of the 20-keV electron flux generated by the shock

was two orders of magnitude smaller than the corresponding flux of electrons accelerated during the flare in the back-sided active region that was inside the field of view of *Ulysses*'s HXR detector. This is consistent with older observations that isolated type II bursts generally occur in the decay phase of HXR bursts. Hence, electron acceleration from coronal shocks is less efficient than impulsive acceleration processes. However, the upper limit of the number of electrons derived by Klein *et al.* (2003) was comparable to the electron numbers inferred by Lin, Mewaldt, and van Hollebeke (1982) for large solar energetic electron events. Therefore their study does not completely rule out the possibility of coronal shocks being the accelerators of electron events in the IP medium.

Several mechanisms have been proposed that enhance the efficiency of shock acceleration. The interaction of a fast CME with a slower previous one has been suggested as a possible mechanism. Gopalswamy *et al.* (2001c) have interpreted the radio enhancement of a faint type II burst in terms of such a scenario: In their event the projected trajectories of the fronts of two CMEs (a slow one and a fast one that was the initial type II's driver) intersect each other and the radio enhancement originated in the same height as the estimated height where the two CMEs interacted. They argued that the radio enhancement was due to shock strengthening when it propagates through the dense material of the slow CME. However, magnetic reconnection, which is obviously required for the penetration of the fast CME into the slower one, could be an alternative explanation for the radio enhancement. Other proposed mechanisms of making shock acceleration more efficient include mirroring by local shock inhomogeneities (Bale *et al.*, 1999) and preacceleration in refracted shocks (Vainio and Khan, 2004).

7.3.2. Electron Acceleration at the Termination Shock of Reconnection Outflows

The reconnection flare model predicts that, in the vicinity of the diffusion region, the slowly inflowing plasma shoots away from the reconnection site as a hot jet. These jets are embedded between a pair of slow magnetosonic shocks. If the jet speed is super-Alfvénic, a fast magnetosonic shock is established by its deceleration, for instance by underlying postflare loops. This shock is called termination shock (TS) and its appearance has been predicted in the numerical simulations by Forbes (1986) and Shibata *et al.* (1995). Tsuneta and Naito (1998) have proposed that it could be the source of the energetic electrons needed for the HXR emission during flares.

Unlike type II bursts, the TS should not show any drift in a dynamic radio spectrum because it is a standing shock. In a couple of events, Aurass, Vršnak, and Mann (2002), Aurass and Mann (2004), and Mann, Aurass, and Warmuth (2006) have identified such spectral radio features in close temporal and spatial association with the flares. In their calculations the TS is considered to energize not only the electrons responsible for the radio emissions but also the electrons needed for the HXR and γ-ray flare emissions (Mann, Aurass, and Warmuth, 2006). The electron acceleration is explained by the relativistically treated shock drift acceleration mechanism in the specific TS geometry.

8. SEPs and Radio Emission

The main locations for electron and ion acceleration in the heliosphere are flare sites and shock waves in the corona and in the IP medium. The energy of these SEP events reaches from a few keV to some GeV. In the 1990s SEP events were classified as either impulsive or gradual (*e.g.*, Reames, 1999) based on the properties of the associated SXR flare,

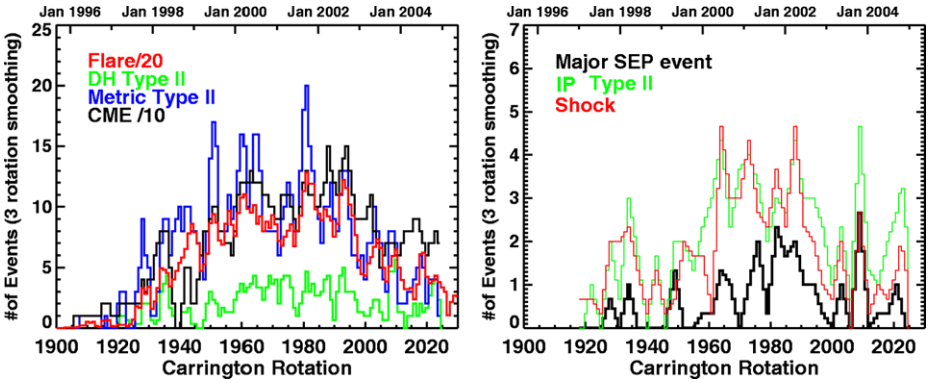

Figure 11 Left: Occurrence rate of metric and DH type II bursts compared with the CME and flare rates. The CME and flare rates are divided by 10 and 20, respectively. Right: Occurrence rate of IP shocks (detected *in situ* by spacecraft), large SEP events (detected by the GOES satellite and defined as those producing a 10-pfu proton event at Earth in the > 10 MeV channel), and IP type II bursts. (From Gopalswamy (2006b); reprinted with permission.)

correlations with radio bursts of type III (impulsive) or types II and IV (gradual), and the presence (gradual) or absence (impulsive) of a CME. Impulsive SEP events were believed to originate in solar flares whereas the energetic particles in gradual SEP events were thought to be accelerated in CME-driven coronal and/or interplanetary shocks. In this scheme the largest SEP events are gradual. Although this classification has been useful, we point out that both flares and CMEs are associated with almost all SEP events, so it is often difficult to distinguish the particle accelerator unambiguously.

8.1. CMEs, Flares, and SEPs

Radio observations have played a key role in realizing that CME-driven shocks contribute to large SEP events. It has been found that there is a 100% association between SEP events and DH type II bursts (Gopalswamy, 2006b) while type II bursts at frequencies below 2 MHz are also associated with large SEP events (Cane and Stone, 1984). Figure 11 indicates that the solar cycle variation of IP shocks, large SEP events, and IP type II bursts is similar, implying that in a statistical sense the three phenomena are closely related. However, Figure 11 shows that the number of SEP events is smaller, but this may be attributed to the fact that SEP events are observed when their source is well connected to the observer. The DH type II bursts are slightly larger in number because even back-sided eruptions can produce them whereas the particles from these eruptions may not arrive at Earth.

It is obvious that CME-driven shocks accelerate particles in the IP medium but it is not at all obvious at what distance from the Sun such acceleration becomes important and up to which energies is effective. Furthermore, SEP events are not associated with CMEs only. Cane, Erickson, and Prestage (2002) showed that several SEP events are associated with type III-*l* bursts (see also Section 3.2.3). To check whether type III-*l* bursts are shock-accelerated or not one has to consider events showing both type II and type III-*l* bursts and check whether the type III-*l* bursts begin at frequencies characteristic of the underlying flare, which are always higher than the nearly simultaneous type II burst starting frequency. Cane, Erickson, and Prestage (2002) presented evidence that this is the case and also noted that, in several SEP events, type III-*l* bursts dominated the radio dynamic spectra. Based on these

arguments they concluded that in their extended database of SEP events the initial acceleration of SEPs does not come from shocks ahead of CMEs but is related to reconnection processes at lower coronal altitudes. The role of CME-driven shocks as primary accelerators of SEPs has been also challenged by Marqué, Posner, and Klein (2006), who showed that in three events with fast CMEs that were not accompanied by metric radio bursts (with the absence of such bursts not attributable to limb occultation), there was no production of any conspicuous SEP event.

8.2. Radio Observations and the Timing of SEP Release

The key to identify the relative importance of flare versus shock acceleration in SEP events is to deduce the location and temporal evolution of the source-emitting particles from the corona into the IP medium. However, the information needed for timing studies of particle injections is washed out by the effects of scattering off magnetic irregularities as the particles travel from the Sun to 1 AU. The detailed magnetic configuration of the inner heliosphere can also come into play (*e.g.*, Larson *et al.*, 1997; Ruffolo *et al.*, 2006). To determine the particle injection profile, it is necessary to deconvolve the effects of particle transport from the particle acceleration sites to the spacecraft. Moreover, it is also imperative to use anisotropy measurements to correctly model the energetic particle transport conditions. However, in most studies (*e.g.*, Lin, 1974; Cliver *et al.*, 1982; Krucker *et al.*, 1999; Klein *et al.*, 1999a; Laitinen *et al.*, 2000; Haggerty and Roelof, 2002) of the determination of the release time, scatter-free propagation is assumed and the time of the release of the particles is regarded as energy independent. Krucker *et al.* (1999) and Haggerty and Roelof (2002) found that the inferred injection time of near relativistic (NR) electrons ($\gtrsim 30$ keV) at the Sun in a few cases is consistent with the timing of the type III radio emission, but in most cases the electrons were apparently released up to half an hour later than the start of the type III burst. The prompt electron events were concentrated in the well-connected area, whereas the delayed events were more spread out. For the origin of the delays three explanations have been proposed: (1) The delayed electrons come from coronal shocks; (2) all electrons originate from a single population, and the delay is due to IP transport effects; and (3) the CME shock front plays a minor role and the delayed electrons originate at a reconnection site behind it (Laitinen *et al.*, 2000; Classen *et al.*, 2003; Maia and Pick, 2004; Klein *et al.*, 2005; Aurass *et al.*, 2006; Maia *et al.*, 2007; for relativistic protons see Akimov *et al.*, 1996; Klein *et al.*, 1999a).

Interpretation (1) has been invoked by Simnett, Roelof, and Haggerty (2002), who showed that the release delays of the NR electrons with respect to the launch times of the associated CMEs tend to anticorrelate with the CME speeds. This trend was interpreted as evidence of electron acceleration by the CME shock at a height of a few solar radii, which is reached sooner if the CME is faster.

Particles from delayed SEP events whose sources are located at the eastern hemisphere cannot reach the Earth directly along the undisturbed IP magnetic field. Krucker *et al.* (1999) studied such SEP events that were accompanied by EIT waves and showed that although the EIT wave itself is too slow to explain the solar release of particles detected *in situ* by shock acceleration in the low corona, the release time can be understood if the particles are accelerated when a three-dimensional wave front intercepts the Earth-connected IP field high in the corona at heliocentric position well away from the flare location.

Interpretation (2) has been used by Cane (2003), Cane and Erickson (2003), and Lintunen and Vainio (2004). Cane (2003) found that the delays increase with the ambient solar

wind density, consistent with the propagation times of the electrons being determined by the characteristics of the IP medium (see also Kahler *et al.*, 2007).

Interpretation (3) has been used for events that show electron release times that coincide closely with the onset of, or changes seen in, long-duration radio emissions. This association supports a scenario in which the particles are accelerated at sites low in the corona, which originate in the wake of the magnetic restructuring linked to the CME development. A similar interpretation has been given to the event of Figure 6 (Maia *et al.*, 2007). A few minutes after the radio event, an impulsive electron event was detected *in situ*. With a detailed transport model for the electron event, Maia *et al.* (2007) obtained an electron injection function at the Sun that was remarkably similar to the radio loop event. The coincidence of the onset and rise phases of the radio loop emission with the presence of the low-altitude radio feature marked with an arrow in Figure 6 suggests that the nonthermal loop electrons (and likely also the *in situ* particles) are accelerated in the disturbed corona behind the CME.

9. Summary and Concluding Remarks

Radio emissions from flares and CMEs provide unique diagnostics of energetic electrons from the low corona to 1 AU. They are a key tool for studying energy release and particle acceleration and transport, detecting the onset and development of CMEs, and constraining the properties of the magnetic field in flare – CME sources as well as the properties of ambient coronal structures. Several important new results have come out recently.

1. Microwave emission from energetic electrons has proved to be a valuable tool in constraining source morphologies and potential acceleration scenarios and in quantitatively assessing the energy spectra of electrons accelerated during flares, especially at higher energies than probed by HXRs. A new window has been opened at wavelengths < 1 mm.
2. Broadband spectral imaging at radio wavelengths has elucidated the formation and early development of CMEs at heights not accessible to coronagraphs. The radio observations indicate interacting magnetic structures of widely different scales or large-scale cavities related to erupting quiescent filaments. The radio data help us understand that CMEs result from the coupling of different spatial scales in the corona that go from current sheets, to active regions and filaments, up to large transequatorial loops.
3. Radio observations at meter and longer wavelengths remain the most direct diagnostic of shock waves in the corona. They continue to provide constraints on their generation, propagation, and basic physical properties and are a key to identify shock wave signatures in EUV images and UV spectra.
4. Meter-wave radio observations are well known to reveal time-extended (minutes to hours) electron acceleration in the corona in long-lasting flares and after the passage of a CME front. It was recently shown that electrons up to relativistic energies can be accelerated in this context; these are revealed by their synchrotron radio emission at decimetric and metric wavelengths. Coherent plasma emission in similar events can be used to probe the coronal magnetic field in a dynamic post-CME configuration.
5. Both shock waves and time-extended particle acceleration are of possible relevance to the injection of energetic particles into space, which can be detected near Earth. The corona probed at decimeter and meter wavelengths is a crucial region for the acceleration and propagation of these particles, and radio diagnostics in this dilute plasma, where collisional radiation processes yielding HXR or γ-ray emission are inefficient, will further play a major role in assessing the origin of SEP events.

The next step toward developing radio diagnostics of coronal explosive phenomena is time-resolved broadband imaging spectroscopy. This requirement will materialize with the development of the Frequency-agile Solar Radio Telescope (FASR; see *e.g.*, Gary, 2006), whose frequency range will cover the solar atmosphere from the chromosphere to the corona out to about $1R_{\odot}$ above the photosphere. The anticipated FASR data combined with joint observations across the electromagnetic spectrum and new *in situ* probes promise exciting new results in the future.

Acknowledgements AN thanks C.E. Alissandrakis, L. Vlahos, and S.M. White for useful discussions and help.

References

Akimov, V.V., Ambrož, P., Belov, A.V., Berlicki, A., Chertok, I.M., Karlický, M., *et al.*: 1996, *Solar Phys.* **166**, 107.
Alissandrakis, C.E.: 1986, *Solar Phys.* **104**, 207.
Alissandrakis, C.E., Preka-Papadema, P.: 1984, *Astron. Astrophys.* **139**, 507.
Alissandrakis, C.E., Nindos, A., Kundu, M.R.: 1993, *Solar Phys.* **147**, 343.
Alissandrakis, C.E., Schadee, A., Kundu, M.R.: 1988, *Astron. Astrophys.* **195**, 290.
Alissandrakis, C.E., Nindos, A., Hilaris, A., Caroublos, C., Arthemis Team: 2005, In: Danesy, D., Poedts, S., De Groof, A., Andries, J. (eds.) *The Dynamic Sun: Challenges for Theory and Observations* **SP-600**, ESA, Noordwijk, 106.1.
Altyntsev, A.T., Grechnev, V.V., Nakajima, H., Fujiki, K., Nishio, M., Prosovetsky, D.V.: 1999, *Astron. Astrophys. Suppl.* **135**, 415.
Altyntsev, A.T., Kuznetsov, A.A., Meshalkina, N.S., Rudenko, G.V., Yan, Y.: 2005, *Astron. Astrophys.* **431**, 1037.
Antiochos, S.K., DeVore, C.R., Klimchuk, J.A.: 1999, *Astrophys. J.* **510**, 485.
Arzner, K., Benz, A.O.: 2005, *Solar Phys.* **231**, 117.
Asai, A., Nakajima, H., Shimojo, M., White, S.M., Hudson, H.S., Lin, R.P.: 2006, *Publ. Astron. Soc. Japan* **58**, 1.
Aschwanden, M.J.: 2002, *Space Sci. Rev.* **101**, 1.
Aschwanden, M.J., Benz, A.O.: 1997, *Astrophys. J.* **480**, 825.
Aschwanden, M.J., Güdel, M.: 1992, *Astrophys. J.* **401**, 736.
Aschwanden, M.J., Benz, A.O., Montello, M.L.: 1994, *Astrophys. J.* **431**, 432.
Aschwanden, M.J., Benz, A.O., Schwartz, R.A.: 1993, *Astrophys. J.* **417**, 790.
Aschwanden, M.J., Wiehl, H.J., Benz, A.O., Kane, S.R.: 1985, *Solar Phys.* **97**, 159.
Aschwanden, M.J., Bastian, T.S., Benz, A.O., Brosius, J.: 1992, *Astrophys. J.* **391**, 380.
Aschwanden, M.J., Benz, A.O., Dennis, B.R., Schwartz, R.A.: 1995, *Astrophys. J.* **455**, 347.
Attrill, G.D.R., Harra, L.K., van Driel-Gesztelyi, L., Démoulin, P.: 2007, *Astrophys. J.* **656**, 101.
Aulanier, G., DeLuca, E.E., Antiochos, S.K., McMullen, R.A., Golub, L.: 2000, *Astrophys. J.* **540**, 1126.
Aurass, H., Klein, K.-L.: 1997, *Astron. Astrophys. Suppl.* **123**, 279.
Aurass, H., Mann, G.: 2004, *Astrophys. J.* **615**, 526.
Aurass, H., Hofmann, A., Urbarz, H.-W.: 1998, *Astron. Astrophys.* **334**, 289.
Aurass, H., Klein, K.-L., Martens, P.C.H.: 1994, *Solar Phys.* **155**, 203.
Aurass, H., Rausche, G., Mann, G.: 2007, *Astron. Astrophys.* **471**, L37.
Aurass, H., Vršnak, B., Mann, G.: 2002, *Astron. Astrophys.* **384**, 273.
Aurass, H., Vourlidas, A., Andrews, M.D., Thompson, B.J., Mann, G.: 1999, *Astrophys. J.* **511**, 451.
Aurass, H., Klein, K.-L., Zlotnik, E.Ya., Zaitsev, V.V.: 2003, *Astron. Astrophys.* **410**, 1001.
Aurass, H., Rausche, G., Mann, G., Hofmann, A.: 2005, *Astron. Astrophys.* **435**, 1137.
Aurass, H., Mann, G., Rausche, G., Warmuth, A.: 2006, *Astron. Astrophys.* **457**, 681.
Bárta, M., Karlický, M.: 2001, *Astron. Astrophys.* **379**, 1045.
Bárta, M., Karlický, M.: 2005, *Astrophys. J.* **631**, 612.
Bárta, M., Karlický, M.: 2006, *Astron. Astrophys.* **450**, 359.
Bale, S.D., Reiner, M.J., Bougeret, J.-L., Kaiser, M.L., Krucker, S., Larson, D.E., Lin, R.P.: 1999, *Geophys. Res. Lett.* **26**, 1573.
Bastian, T.S.: 1994, *Astrophys. J.* **426**, 774.
Bastian, T.S., Benz, A.O., Gary, D.E.: 1998, *Ann. Rev. Astron. Astrophys.* **36**, 131.

Bastian, T.S., Fleishman, G.D., Gary, D.E.: 2007, *Astrophys. J.* **666**, 1256.
Bastian, T.S., Pick, M., Kerdraon, A., Maia, D., Vourlidas, A.: 2001, *Astrophys. J.* **558**, L65.
Benz, A.O.: 1985, *Solar Phys.* **96**, 357.
Benz, A.O.: 1986, *Solar Phys.* **104**, 99.
Benz, A.O.: 1993, *Plasma Astrophysics, Kinetic Processes in Solar and Stellar Coronae*, Kluwer, Dordrecht.
Benz, A.O., Jaeggi, M., Zlobec, P.: 1982, *Astron. Astrophys.* **109**, 305.
Benz, A.O., Saint-Hilaire, P., Vilmer, N.: 2002, *Astron. Astrophys.* **383**, 678.
Benz, A.O., Treumann, R., Vilmer, N., Mangeney, A., Pick, M., Raoult, A.: 1982, *Astron. Astrophys.* **108**, 161.
Benz, A.O., Barrow, C.H., Dennis, B.R., Pick, M., Raoult, A., Simnett, G.: 1983, *Solar Phys.* **83**, 267.
Benz, A.O., Grigis, P.C., Csillaghy, A., Saint-Hilaire, P.: 2005, *Solar Phys.* **226**, 121.
Bernold, T., Treumann, R.: 1983, *Astrophys. J.* **264**, 677.
Biesecker, D.A., Myers, D.C., Thompson, B.J., Hammer, D.M., Vourlidas, A.: 2002, *Astrophys. J.* **569**, 1009.
Bone, L., Brown, J.C., Fletcher, L., Veronig, A., White, S.: 2007, *Astron. Astrophys.* **466**, 339.
Bruggmann, G., Vilmer, N., Klein, K.-L., Kane, S.R.: 1994, *Solar Phys.* **149**, 171.
Cane, H.V.: 2003, *Astrophys. J.* **598**, 1403.
Cane, H.V., Erickson, W.C.: 2003, *J. Geophys. Res.* **108**, 1203.
Cane, H.V., Erickson, W.C.: 2005, *Astrophys. J.* **623**, 1180.
Cane, H.V., Stone, R.G.: 1984, *Astrophys. J.* **282**, 339.
Cane, H.V., Erickson, W.C., Prestage, N.P.: 2002, *J. Geophys. Res. A* **107**(10), 1315.
Cane, H.V., Stone, R.G., Fainberg, J., Steinberg, J.L., Hoang, S., Stewart, R.D.: 1981, *Geophys. Res. Lett.* **8**, 1285.
Caroubalos, C., Poquérusse, M., Steinberg, J.-L.: 1974, *Astron. Astrophys.* **32**, 255.
Chernov, G.P., Yan, Y.H., Fu, Q.J.: 2003, *Astron. Astrophys.* **406**, 1071.
Chernov, G.P., Sych, R.A., Yan, Y., Fu, Q., Tan, C., Huang, G., Wang, D.Y., Wu, H.: 2006, *Solar Phys.* **237**, 397.
Cho, K.-S., Lee, J., Gary, D.E., Moon, Y.-J., Park, Y.D.: 2007, *Astron. Astrophys.* **461**, 1121.
Chertok, I.M., Kahler, S., Aurass, H., Gnezdilov, A.A.: 2001, *Solar Phys.* **202**, 337.
Classen, H.T., Aurass, H.: 2002, *Astron. Astrophys.* **384**, 1098.
Classen, H.T., Mann, G., Klassen, A., Aurass, H.: 2003, *Astron. Astrophys.* **409**, 309.
Cliver, E.W., Webb, D.F., Howard, R.A.: 1999, *Solar Phys.* **187**, 89.
Cliver, E.W., Kahler, S.W., Shea, M.A., Smart, D.F.: 1982, *Astrophys. J.* **260**, 362.
Cohen, M.: 1960, *Astrophys. J.* **131**, 664.
Dauphin, C., Vilmer, N., Krucker, S.: 2006, *Astron. Astrophys.* **455**, 339.
Delannée, C., Aulanier, G.: 1999, *Solar Phys.* **190**, 107.
Dulk, G.A., Leblanc, Y., Bastian, T.S., Bougeret, J.-L.: 2000, *J. Geophys. Res. A* **105**(12), 27343.
Duncan, R.A.: 1979, *Solar Phys.* **63**, 389.
Elgarøy, E.O.: 1959, *Nature*, 184, 885.
Elgarøy, E.O.: 1977, *Solar Noise Storms*, Pergamon, Oxford.
Fainberg, J., Stone, R.G.: 1974, *Space Sci. Rev.* **16**, 145.
Fleishman, G.D., Melnikov, V.F.: 1998, *Phys.-Usp.* **41**, 1157.
Fleishman, G.D., Melnikov, V.F.: 2003a, *Astrophys. J.* **584**, 1071.
Fleishman, G.D., Melnikov, V.F.: 2003b, *Astrophys. J.* **587**, 823.
Fleishman, G.D., Gary, D.E., Nita, G.M.: 2003, *Astrophys. J.* **593**, 571.
Fleishman, G.D., Nita, G.M., Gary, D.E.: 2005, *Astrophys. J.* **620**, 506.
Forbes, T.G.: 1986, *Astrophys. J.* **305**, 553.
Gary, D.E.: 2006, In: *Proceedings of Nobeyama Symposium 2004*, 121.
Gary, D.E., Dulk, G.A., House, L., Illing, R., Sawyer, C., Wagner, W.J., McLean, D.J., Hildner, E.: 1984, *Astron. Astrophys.* **134**, 222.
Ginzburg, V.L., Frank, I.M.: 1946, *Z. Eksp. Teor. Fiz.* **16**, 15.
Goff, C.P., van Driel-Gesztelyi, L., Démoulin, P., Culhane, J.L., Matthews, S.A., Harra, L.K., *et al.*: 2007, *Solar Phys.* **240**, 283.
Gopalswamy, N.: 2006a, In: *Proceedings of Nobeyama Symposium 2004*, 81.
Gopalswamy, N.: 2006b. In: Gopalswamy, N., Mewaldt, R., Torsti, J. (eds.) *Solar Eruptions and Energetic Particles*, *Geophys. Mon. Ser.* **165**, AGU, Washington, 207.
Gopalswamy, N., Hanaoka, Y.: 1998, *Astrophys. J.* **498**, L179.
Gopalswamy, N., Kundu, M.R.: 1992, *Astrophys. J.* **390**, L37.
Gopalswamy, N., Kundu, M.R., Hanaoka, Y., Enome, S., Lemen, J.R., Akioka, M.: 1996, *New Astron.* **1**, 207.
Gopalswamy, N., Kaiser, M.L., Lepping, R.P., Kahler, S.W., Ogilvie, K., Berdichevsky, D., Kondo, T., Isobe, T., Akioka, M.: 1998, *J. Geophys. Res.* **103**, 307.

Gopalswamy, N., Shibasaki, K., Thompson, B.J., Gurman, J., DeForest, C.J.: 1999, *Geophys. Res. Lett.* **104**, 9767.
Gopalswamy, N., Lara, A., Kaiser, M.L., Bougeret, J.-L.: 2001a, *J. Geophys. Res.* **106**, 25261.
Gopalswamy, N., St. Syr, O.C., Kaiser, M.L., Yashiro, S.: 2001b, *Solar Phys.* **203**, 149.
Gopalswamy, N., Yashiro, S., Kaiser, M.L., Howard, R.A., Bougeret, J.-L.: 2001c, *Astrophys. J.* **548**, L91.
Gopalswamy, N., Shimojo, M., Lu, W., Yashiro, S., Shibasaki, K., Howard, R.A.: 2003, *Astrophys. J.* **586**, 562.
Grechnev, V.V., Kundu, M., Nindos, A.: 2006, *Publ. Astron. Soc. Japan* **58**, 47.
Grechnev, V.V., Uralov, A.M., Zandanov, V.G., Baranov, N.Y., Shibasaki, K.: 2006, *Publ. Astron. Soc. Japan* **58**, 69.
Gurnett, D.A., Baumback, M.M., Rosenbauer, H.: 1978, *J. Geophys. Res.* **83**, 616.
Green, L.M., Matthews, S.A., van Driel-Gesztelyi, L., Harra, L.K., Culhane, J.L.: 2002, *Solar Phys.* **205**, 325.
Haggerty, D.K., Roelof, E.C.: 2002, *Astrophys. J.* **579**, 841.
Hanaoka, Y.: 1996, *Solar Phys.* **165**, 275.
Hanaoka, Y.: 1997, *Solar Phys.* **173**, 319.
Hanaoka, Y.: 1999, In: Bastian, T.S., Gopalswamy, N., Shibasaki, K. (eds.) *Proceedings of the Nobeyama Symposium, Kiyosato, Japan, 27–30 October 1998*, 153.
Hanaoka, Y., Kurokawa, H., Enome, S., Nakajima, H., Shibasaki, K., Nishio, M., *et al.*: 1994, *Publ. Astron. Soc. Japan* **46**, 205.
Harrison, R.A.: 1995, *Astron. Astrophys.* **304**, 585.
Hillaris, A., Alissandrakis, C.E., Bougeret, J.-L., Caroubalos, C.: 1999, *Astron. Astrophys.* **342**, 271.
Hoang, S., Lacombe, C., MacDowall, R.J., Thejappa, G.: 2007, *J. Geophys. Res.* **112**, 9102.
Hori, K.: 2000, *Astrophys. J.* **543**, 1011.
Hori, K., Culhane, J.L.: 2002, *Astron. Astrophys.* **382**, 666.
Hudson, H.S., Kosugi, T., Nitta, N., Shimojo, M.: 2001, *Astrophys. J.* **561**, L211.
Isliker, H.: 1996, *Astron. Astrophys.* **310**, 672.
Isliker, H., Benz, A.O.: 1994, *Astron. Astrophys.* **104**, 145.
Kahler, S.W., Hundhausen, A.J.: 1992, *J. Geophys. Res.* **97**, 1619.
Kahler, S.W., Cliver, E.W., Cane, H.V.: 1989, *Solar Phys.* **120**, 393.
Kahler, S.W., Aurass, H., Mann, G., Klassen, A.: 2007, *Astrophys. J.* **656**, 567.
Kai, K.: 1970, *Solar Phys.* **11**, 310.
Kai, K., Melrose, D.B., Suzuki, S.: 1985, In: McLean, D.J., Labrum, N.R. (eds.) *Solar Radiophysics*, Cambridge University Press, Cambridge, 415.
Karlický, M.: 2004, *Astron. Astrophys.* **417**, 325.
Karlický, M., Bárta, M.: 2007, *Adv. Space Res.* **39**, 1415.
Karlický, M., Kosugi, T.: 2004, *Astron. Astrophys.* **419**, 1159.
Karlický, M., Fárník, F., Mészárosová, H.: 2002, *Astron. Astrophys.* **395**, 677.
Kathiravan, C., Ramesh, R., Subramanian, K.R.: 2002, *Astrophys. J.* **567**, L93.
Kaufmann, P., Raulin, J.-P., Correia, E., Costa, J.E.R., Giménez de Castro, C.G., Silva, A.V.R., *et al.*: 2001, *Astrophys. J.* **548**, L95.
Kaufmann, P., Raulin, J.-P., Giménez de Castro, C.G., Levato, H., Gary, D.E., Costa, J.E.R., *et al.*: 2004, *Astrophys. J.* **603**, L121.
Kaufmann, P., Trottet, G., Giménez de Castro, C., Raulin, J., Gary, D., Fernandez, G., *et al.*: 2007, *Bull. Am. Astron. Soc.* **210**, 93.30.
Khan, J.I., Aurass, H.: 2002, *Astron. Astrophys.* **383**, 1018.
Khan, J.I., Aurass, H.: 2006, *Astron. Astrophys.* **457**, 319.
Khan, J.I., Vilmer, N., Saint-Hilaire, P., Benz, A.O.: 2002, *Astron. Astrophys.* **388**, 363.
Klassen, A., Pohjolainen, S., Klein, K.-L.: 2003, *Solar Phys.* **218**, 197.
Klassen, A., Aurass, H., Klein, K.-L., Hofmann, A., Mann, G.: 1999, *Astron. Astrophys.* **343**, 287.
Klassen, A., Aurass, H., Mann, G., Thompson, B.J.: 2000, *Astron. Astrophys. Suppl.* **141**, 357.
Klein, K.-L.: 1992, In: Marsch, E., Schwenn, R. (eds.) *Solar Wind Seven*, Pergamon, Oxford, 635.
Klein, K.-L.: 2005, *Adv. Space Res.* **35**, 1759.
Klein, K.-L., Trottet, G.: 1984, *Astron. Astrophys.* **141**, 67.
Klein, K.-L., Chupp, E.L., Trottet, G., Magun, A., Dunphy, P.P., Rieger, E., Urpo, S.: 1999a, *Astron. Astrophys.* **348**, 271.
Klein, K.-L., Khan, J.I., Vilmer, N., Delouis, J.-M., Aurass, H.: 1999b, *Astron. Astrophys.* **346**, L53.
Klein, K.-L., Trottet, G., Lantos, P., Delaboudinière, J.-P.: 2001, *Astron. Astrophys.* **373**, 1073.
Klein, K.-L., Schwartz, R.A., McTiernan, J.M., Trottet, G., Klassen, A., Lecacheux, A.: 2003, *Astron. Astrophys.* **410**, 1001.
Klein, K.-L., Krucker, S., Trottet, G., Hoang, S.: 2005, *Astron. Astrophys.* **431**, 1047.

Kliem, B., Karlický, M., Benz, A.O.: 2000, *Astron. Astrophys.* **360**, 715.
Kolomanski, S., Tomczak, M., Ronowicz, P., Karlický, M., Aurass, H.: 2007, *Cent. Eur. Astrophys. Bull.* **31**, 125.
Krucker, S., Larson, D.E., Lin, R.P., Thompson, B.J.: 1999, *Astrophys. J.* **519**, 864.
Kuijpers, J.: 1975, *Solar Phys.* **44**, 173.
Kuijpers, J., van der Post, P., Slottje, C.: 1981, *Astron. Astrophys.* **103**, 331.
Kundu, M.R., Vlahos, L.: 1982, *Space Sci. Rev.* **32**, 405.
Kundu, M.R., MacDowall, R.J., Stone, R.G.: 1990, *Astrophys. Space Sci.* **165**, 101.
Kundu, M.R., Nindos, A., Grechnev, V.V.: 2004, *Astron. Astrophys.* **420**, 351.
Kundu, M.R., Schmahl, E.J., Velusamy, T., Vlahos, L.: 1982, *Astron. Astrophys.* **108**, 188.
Kundu, M.R., White, S.M., Gopalswamy, N., Lim, J.: 1994, *Astrophys. J. (Suppl.)* **90**, 599.
Kundu, M.R., Nitta, N., White, S.M., Shibasaki, K., Enome, S., Sakao, T., Kosugi, T., Sakurai, T.: 1995, *Astrophys. J.* **454**, 522.
Kundu, M.R., Nindos, A., Vilmer, N., Klein, K.-L., Shibata, K., Ohyama, M.: 2001a, *Astrophys. J.* **559**, 443.
Kundu, M.R., Nindos, A., White, S.M., Grechnev, V.V.: 2001b, *Astrophys. J.* **557**, 880.
Kundu, M.R., White, S.M., Shibasaki, K., Sakurai., T., Grechnev, V.V.: 2001c, *Astrophys. J.* **547**, 1090.
Kundu, M.R., Garaimov, V.I., White, S.M., Krucker, S.: 2004, *Astrophys. J.* **600**, 1052.
LaBelle, J., Treumann, R.A., Yoon, P.H., Karlický, M.: 2003, *Astrophys. J.* **593**, 1195.
Laitinen, T., Klein, K.-L., Kocharov, L., Torsti, J., Trottet, G., Bothmer, V., Kaiser, M.L., Rank, G., Reiner, M.J.: 2000, *Astron. Astrophys.* **360**, 729.
Lantos, P., Kerdraon, A., Rapley, G.G., Bentley, R.D.: 1981, *Astron. Astrophys.* **101**, 33.
Larson, D.E., Lin, R.P., Ergun, R.E., McTiernan, J.M., McFadden, J.P., Carlson, C.W., *et al.*: 1997, *Adv. Space Res.* **20**, 655.
Lecacheux, A., Steiberg, J.-L., Hoang, S., Dulk, G.A.: 1989, *Astron. Astrophys.* **217**, 237.
Ledenev, V.G., Yan, Y.-H., Fu, Q.-J.: 2001, *Chin. J. Astron. Astrophys.* **1**, 475.
Leblanc, Y., Dulk, G.A., Vourlidas, A., Bougeret, J.-L.: 2001, *J. Geophys. Res.* **106**, 25301.
Lee, J., Gary, D.E.: 2000, *Astrophys. J.* **543**, 457.
Lee, J., Gary, D.E., Shibasaki, K.: 2000, *Astrophys. J.* **531**, 1109.
Lee, J., Gary, D.E., Qiu, J., Gallagher, P.: 2002, *Astrophys. J.* **572**, 609.
Lin, R.P.: 1974, *Space Sci. Rev.* **16**, 189.
Lin, R.P., Mewaldt, R.A., van Hollebeke, M.A.I.: 1982, *Astrophys. J.* **253**, 949.
Lingenfelter, R.E., Ramaty, R.: 1967, *Planet. Space Sci.* **15**, 1303.
Lintunen, J., Vainio, R.: 2004, *Astron. Astrophys.* **420**, 343.
Low, B.C., Hundhausen, J.R.: 1995, *Astrophys. J.* **443**, 818.
Lüthi, T., Lüdi, A., Magun, A.: 2004, *Astron. Astrophys.* **420**, 361.
Lüthi, T., Magun, A., Miller, M.: 2004, *Astron. Astrophys.* **415**, 1123.
MacDowall, R.J., Stone, R.G., Kundu, M.R.: 1987, *Solar Phys.* **111**, 397.
Maia, D., Pick, M.: 2004, *Astrophys. J.* **609**, 1082.
Maia, D., Pick, M., Kerdraon, A., Howard, R., Brueckner, G.E., Michels, D.J., *et al.*: 1998, *Solar Phys.* **181**, 121.
Maia, D., Pick, M., Vourlidas, A., Howard, R.: 2000, *Astrophys. J.* **528**, L49.
Maia, D., Aulanier, G., Wang, S.J., Pick, M., Malherbe, J.-M.: 2003, *Astrophys. J.* **405**, 313.
Maia, D., Gama, R., Mercier, C., Pick, M., Kerdraon, A., Karlický, M.: 2007, *Astrophys. J.* **660**, 874.
Mancuso, S., Raymond, J.C.: 2004, *Astron. Astrophys.* **413**, 363.
Manoharan, P.K., Kundu, M.R.: 2003, *Astrophys. J.* **592**, 597.
Mann, G.: 1995, In: Benz, A.O., Kruger, A. (eds.) *Coronal Magnetic Energy Releases*, Springer, Berlin, 183.
Mann, G., Klassen, A.: 2002, In: Kuijpers, J. (ed.) *Solar Variability: From Core to Outer Frontiers* **SP-506**, ESA, Nordwijk, 245.
Mann, G., Motschmann, U.: 1987, *Solar Phys.* **110**, 381.
Mann, G., Classen, T., Aurass, H.: 1995, *Astron. Astrophys.* **295**, 775.
Mann, G., Aurass, H., Warmuth, A.: 2006, *Astron. Astrophys.* **454**, 969.
Mann, G., Baumgartel, K., Chernov, G.P., Karlický, M.: 1989, *Solar Phys.* **120**, 383.
Mann, G., Aurass, H., Klassen, A., Estel, C., Thompson, B.J.: 1999, In: Vial, J.-C., Kaldeich-Schurmann, B. (eds.) *Plasma Dynamics and Diagnostics in the Solar Transition Region and Corona* **SP-446**, ESA, Nordwijk, 477
Mann, G., Klassen, A., Aurass, H., Classen, H.-T.: 2003, *Astron. Astrophys.* **400**, 329.
Marqué, C., Lantos, P., Delaboudinière, J.-P.: 2002, *Astron. Astrophys.* **387**, 317.
Marqué, C., Posner, A., Klein, K.-L.: 2006, *Astrophys. J.* **642**, 1222.
Melnikov, V.F., Magun, A.: 1998, *Solar Phys.* **178**, 153.
Melnikov, V.F., Shibasaki, K., Reznikova, V.E.: 2002, *Astrophys. J.* **580**, L185.
Melrose, D.B.: 1987, *Solar Phys.* **111**, 89.

Melrose, D.B.: 1997, *Astrophys. Space Sci.* **242**, 209.
Melrose, D.B., Robinson, P.A., Feletto, T.M.: 1995, *Solar Phys.* **158**, 139.
Mercier, C.: 1996, *Ann. Geophys.* **14**, 42.
Nelson, G.J., Melrose, D.B.: 1985, In: McLean, D.J., Labrum, N.R. (eds.) *Solar Radiophysics*, Cambridge University Press, Cambridge, 333
Nelson, G.J., Robinson, R.D.: 1975, *Publ. Astron. Soc. Aust.* **2**, 370.
Nindos, A., Aurass, H.: 2007, In: Klein, K.-L., MacKinnon, A.L. (eds.) *The High Energy Corona: Waves, Eruptions, Particles*, *Lecture Notes in Physics* **725**, Springer, Berlin, 251.
Nindos, A., White, S.M., Kundu, M.R., Gary, D.E.: 2000, *Astrophys. J.* **533**, 1053.
Nishio, M., Yaji, K., Kosugi, T., Nakajima, H., Sakurai, T.: 1997, *Astrophys. J.* **489**, 976.
Nita, G.M., Gary, D.E., Lee, J.: 2004, *Astrophys. J.* **605**, 528.
Paesold, G., Benz, A.O., Klein, K.-L., Vilmer, N.: 2001, *Astron. Astrophys.* **371**, 333.
Platonov, K.Yu., Fleishman, G.D.: 1994, *Z. Eksp. Teor. Fiz.* **79**, 572.
Pick, M., Maia, D.: 2005, *Adv. Space Res.* **35**, 1876.
Pick, M., van den Oord, G.H.: 1990, *Solar Phys.* **130**, 83.
Pohjolainen, S., Maia, D., Pick, M., Vilmer, N., Khan, J.I., Otruba, W., Warmuth, A., Benz, A., Alissandrakis, C., Thompson, B.J.: 2001, *Astrophys. J.* **556**, 421.
Pohjolainen, S., Vilmer, N., Khan, J.I., Hillaris, A.: 2005, *Astron. Astrophys.* **434**, 329.
Poquérusse, M., Steinberg, J.-L., Caroubalos, C., Dulk, G.A., MacQueen, R.M.: 1988, *Astron. Astrophys.* **192**, 323.
Poquérusse, M., Hoang, S., Bougeret, J.-L., Moncuquet, M.: 1995, In: *Solar Wind 8 Proc., Dana Point/California*, 62.
Potter, D.W., Lin, R.P., Anderson, K.A.: 1980, *Astrophys. J.* **236**, 97.
Preka-Papadema, P., Alissandrakis, C.E.: 1988, *Astron. Astrophys.* **191**, 365.
Preka-Papadema, P., Alissandrakis, C.E.: 1992, *Astron. Astrophys.* **257**, 307.
Ramaty, R.: 1969, *Astrophys. J.* **158**, 753.
Ramesh, R., Kathiravan, C., Narayan, A.S., Ebenezer, E.: 2003, *Astron. Astrophys.* **400**, 753.
Raoult, A., Pick, M., Dennis, B.R., Kane, S.R.: 1985, *Astrophys. J.* **299**, 1027.
Raulin, J.-P., Kundu, M.R., Hudson, H.S., Nitta, N., Raoult, A.: 1996, *Astron. Astrophys.* **306**, 299.
Raulin, J.-P., White, S.M., Kundu, M.R., Silva, A.V.R., Shibasaki, K.: 1999, *Astrophys. J.* **522**, 547.
Rausche, G., Aurass, H., Mann, G., Karlický, M., Vocks, C.: 2007, *Solar Phys.* **245**, 327.
Raymond, J.C., Thompson, B.J., St. Cyr, O.C., Gopalswamy, N., Kahler, S., Kaiser, M., *et al.*: 2000, *Geophys. Res. Lett.* **27**, 1439.
Reames, D.: 1999, *Space Sci. Rev.* **90**, 413.
Reiner, M.J., Anderson, K.A., Roelof, E., Armstrong, T., Hospodarsky, G.B., Fainberg, J., *et al.*: 1995, *Space Sci. Rev.* **72**, 261.
Reiner, M.J., Karlický, M., Jiřička, K., Aurass, H., Mann, G., Kaiser, M.L.: 2000, *Astrophys. J.* **530**, 1049.
Reiner, M.J., Kaiser, M.L., Karlický, M., Jiřička, K., Bougeret, J.-L.: 2001, *Solar Phys.* **204**, 121.
Robinson, R.D.: 1985, In: McLean, D.J., Labrum, N.R. (eds.) *Solar Radiophysics*, Cambridge University Press, Cambridge, 385.
Robinson, R.D., Benz, A.O.: 2000, *Solar Phys.* **194**, 345.
Robinson, R.D., Cairns, I.H., Gurnett, D.A.: 1992, *Astrophys. J.* **387**, L101.
Ruffolo, D., Tooprakai, P., Rujiwarodom, M., Khumlumlert, T., Wechakama, M., Bieber, J.W., *et al.*: 2006, *Astrophys. J.* **639**, 1186.
Sakai, J.I., Nagasugi, Y.: 2007, *Astron. Astrophys.* **470**, 1117.
Shanmugaraju, A., Moon, Y.-J., Cho, K.-S., Dryer, M., Umapathy, S.: 2006, *Solar Phys.* **233**, 117.
Sheridan, K.V., Jackson, B.V., McLear, D.J., Dulk, G.A.: 1978, *Proc. Astron. Soc. Austr.* **3**, 249.
Shibata, K., Masuda, S., Shimojo, M., Hara, H., Yokoyama, T., Tsuneta, S., *et al.*: 1995, *Astrophys. J.* **451**, L83.
Silva, A.V.R., Wang, H., Gary, D.E.: 2000, *Astrophys. J.* **545**, 1116.
Silva, A.V.R., Share, G.H., Murphy, R.J., Costa, J.E.R., Giménez de Castro, C.G., Raulin, J.-P., Kaufmann, P.: 2007, *Solar Phys.* **245**, 311.
Simnett, G.M., Roelof, E.C., Haggerty, D.K.: 2002, *Astrophys. J.* **579**, 854.
Somov, B., Kosugi, T.: 1997, *Astrophys. J.* **485**, 859.
Steinberg, J.-L., Hoang, S., Lecacheux, A., Aubier, M.G., Dulk, G.A.: 1984, *Astron. Astrophys.* **140**, 39.
Steinolfson, R.S.: 1984, *Solar Phys.* **94**, 193.
Steinolfson, R.S.: 1985, In: Tsurutani, B.T., Stone, R.G. (eds.) *Collisionless Shocks in the Heliosphere: Reviews of Current Research*, *Geophys. Mon. Ser.* **35**, AGU, Washington, 1.
Stepanov, A.V., Kliem, B., Kruger, A., Hildebrandt, J., Garaimov, V.I.: 1999, *Astrophys. J.* **524**, 961.
Stepanov, A.V., Yokoyama, T., Shibasaki, K., Melnikov, V.F.: 2007, *Astron. Astrophys.* **465**, 706.
Stewart, R.T.: 1984, *Solar Phys.* **94**, 379.

Stewart, R.T.: 1985, In: McLean, D.J., Labrum, N.R. (eds.) *Solar Radiophysics*, Cambridge University Press, Cambridge, 361.
Tajima, T., Benz, A.O., Thaker, M., Leboeuf, J.N.: 1990, *Astron. Astrophys.* **353**, 666.
Temmer, M., Veronig, A.M., Vršnak, B., Miklenic, C.: 2007, *Astrophys. J.* **654**, 665.
Treumann, R.A., Güdel, M., Benz, A.O.: 1990, *Astron. Astrophys.* **236**, 242.
Trottet, G., Vilmer, N.: 1984, *Adv. Space Res.* **4**, 153.
Trottet, G., Pick, M., House, L., Illing, R., Sawyer, C., Wagner, W.: 1982, *Astron. Astrophys.* **111**, 306.
Trottet, G., Vilmer, N., Barat, C., Benz, A., Magun, A., Kuznetsov, A., Sunyaev, R., Terekhov, O.: 1998, *Astron. Astrophys.* **334**, 1099.
Trottet, G., Rolli, E., Magun, A., Barat, C., Kuznetsov, A., Sunyaev, R., Terekhov, O.: 2000, *Astron. Astrophys.* **356**, 1067.
Trottet, G., Raulin, J.-P., Kaufmann, P., Siarkowski, M., Klein, K.-L., Gary, D.E.: 2002, *Astron. Astrophys.* **381**, 694.
Trottet, G., Krucker, S., Lüthi, T., Magun, A.: 2008, *Astrophys. J.* **678**, 509.
Tsuneta, S., Naito, T.: 1998, *Astrophys. J.* **495**, L67.
Uchida, Y.: 1968, *Solar Phys.* **4**, 30.
Uchida, Y., Altschuler, M.D., Newkirk, G.: 1973, *Solar Phys.* **28**, 495.
Uralov, A.M., Lesovoi, S.V., Zandanov, V.G., Grechnev, V.V.: 2002, *Solar Phys.* **208**, 69.
Vainio, R., Khan, J.I.: 2004, *Astrophys. J.* **600**, 451.
Veronig, A.M., Brown, J.C.: 2004, *Astrophys. J.* **603**, L117.
Veronig, A.M., Brown, J.C., Dennis, B.R., Schwartz, R.A., Sui, L., Tolbert, A.K.: 2005, *Astrophys. J.* **621**, 482.
Veronig, A.M., Karlický, M., Vršnak, B., Temmer, M., Magdalenic, J., Dennis, B.R., Otruba, W., Pötzi, W.: 2006, *Astron. Astrophys.* **446**, 675.
Vlahos, L.: 1994, *Space Sci. Rev.* **68**, 39.
Vlahos, L., Raoult, A.: 1995, *Astron. Astrophys.* **296**, 844.
Vlahos, L., Georgoulis, M., Kluiving, R., Paschos, P.: 1995, *Astron. Astrophys.* **299**, 897.
Vršnak, B., Lulic, S.: 2000, *Solar Phys.* **196**, 157.
Vršnak, B., Aurass, H., Magdalenic, J., Gopalswamy, N.: 2001, *Astron. Astrophys.* **377**, 321.
Vršnak, B., Warmuth, A., Temmer, M., Veronig, A., Magdalenic, J., Hillaris, A., Karlický, M.: 2006, *Astron. Astrophys.* **448**, 739.
Wagner, W.J., MacQueen, R.M.: 1983, *Astron. Astrophys.* **120**, 136.
Wagner, W.J., Hildner, E., House, L.L., Sawyer, C., Sheridan, K.V., Dulk, G.A.: 1981, *Astrophys. J.* **244**, L123.
Wang, S., Yan, Y., Zhao, R., Fu, Q., Tan, C., Xu, L., Wang, S., Lin, H.: 2001, *Solar Phys.* **204**, 153.
Warmuth, A. 2007, In: Klein, K.-L., MacKinnon, A. (eds.) *The High-Energy Solar Corona: Waves, Eruptions, Particles*, *Lecture Notes in Physics*, **725**, Springer, Berin, 107.
Warmuth, A., Mann, G.: 2005, *Astron. Astrophys.* **435**, 1123.
Warmuth, A., Vršnak, B., Magdalenic, J., Hanslmeier, A., Otruba, W.: 2004, *Astron. Astrophys.* **418**, 1101.
White, S.M., Kundu, M.R., Garaimov, V.I., Yokoyama, T., Sato, J.: 2002, *Astrophys. J.* **576**, 505.
White, S.M., Krucker, S., Shibasaki, K., Yokoyama, T., Shimojo, M., Kundu, M.R.: 2003, *Astrophys. J.* **595**, L111.
Yan, Y., Pick, M., Wang, M., Krucker, S., Vourlidas, A.: 2006, *Solar Phys.* **239**, 277.
Yokoyama, T., Nakajima, H., Shibasaki, K., Melnikov, V.F., Stepanov, A.V.: 2002, *Astrophys. J.* **576**, L87.
Zhang, J., Dere, K.P., Howard, R.A., Kundu, M.R., White, S.M.: 2001, *Astrophys. J.* **559**, 452.
Zheleznyakov, V.V.: 1970, *Radio Emission of the Sun and Planets*, Pergamon, New York.
Zheleznyakov, V.V., Zlotnik, E.Ya.: 1975, *Solar Phys.* **43**, 431.
Zlotnik, E.Ya.: 1981, *Astron. Astrophys.* **101**, 250.
Zlotnik, E.Ya., Zaitsev, V.V., Aurass, H., Mann, G., Hofmann, A.: 2003, *Astron. Astrophys.* **410**, 1011.